European Journal of Pharmaceutical Sciences 173 (2022) 106184

Contents lists available at ScienceDirect

European Journal of Pharmaceutical Sciences

journal homepage: www.elsevier.com/locate/ejps

Novel cyclic C_5-curcuminoids penetrating the blood-brain barrier: Design, synthesis and antiproliferative activity against astrocytoma and neuroblastoma cells

Imre Huber [a,*], Edina Pandur [b], Katalin Sipos [b], Lilla Barna [c], András Harazin [c], Mária A. Deli [c], Levente Tyukodi [a], Gergely Gulyás-Fekete [d], Győző Kulcsár [a], Zsuzsanna Rozmer [a]

[a] Department of Pharmaceutical Chemistry, University of Pécs, Pécs, Hungary
[b] Department of Pharmaceutical Biology, University of Pécs, Pécs, Hungary
[c] Biological Barriers Research Group, Institute of Biophysics, Biological Research Centre, Hungarian Academy of Sciences, Szeged, Hungary
[d] University of Pécs, Department of Biochemistry and Medical Chemistry, Pécs, Hungary

ARTICLE INFO

Keywords:
Curcuminoids
Antiproliferative
Selective cytotoxicity
logP_{TLC}
Albumin binding
Blood-brain barrier

ABSTRACT

Novel series of cyclic C_5-curcuminoids **17a-j** and **19-22** were prepared as cytotoxic agents and evaluated against human neuroblastoma (SH-SY5Y) or human grade IV astrocytoma (CCF-STTG1) cell lines in low (~0.1 nM - 10 nM) concentrations. Among the tested 21 derivatives, 16 displayed potent antiproliferative activity with IC_{50} values in the low nanomolar to picomolar range (IC_{50} = 7.483-0.139 nM). Highly active compounds like N-monocarboxylic derivative **19b** with IC_{50} = 0.139 nM value against neuroblastoma and N-alkyl substituted **11** with IC_{50} = 0.257 nM against astrocytoma proved some degree of selectivity toward non-cancerous astrocytes and kidney cells. This potent anticancer activity did not show a strong correlation with experimental logP_{TLC} values, but the most potent antiproliferative molecules **11-13** and **19-22** are belonging to discrete subgroups of the cyclic C_5-curcuminoids. Compounds **12, 17c** and **19b** were subjected to blood-brain barrier (BBB) penetration studies, too. The BBB was revealed to be permeable for all of them but, as the apparent permeability coefficient (P_{app}) values mirrored, in different ratios. Lower toxicity of **12, 17c** and **19b** was observed toward primary rat brain endothelial cells of the BBB model, which means they remained undamaged under 10 μM concentrations. Penetration depends, at least in part, on albumin binding of **12, 17c** and **19b** and the presence of monocarboxylic acid transporters in the case of **19b**. Permeation through the BBB and albumin binding, we described here, is the first example of cyclic C_5-curcuminoids as to our knowledge.

1. Introduction

Herbal and other natural model compounds are unbeatable and, in many cases, inevitable sources of lead molecules and drug candidates in pharmaceutical research (Koehn and Carter, 2005). The long history of turmeric, first as a popular nutraceutical and then a pharmaceutical, is such a remarkable example. Plants in the *Zingiberaceae* (ginger) family has been used for thousands of years to prepare turmeric, as an intense yellow powder from the dried rhizome (subterranean stem) of species like *Curcuma longa L.* and *Curcuma domestica L.* Isolation of the active ingredients from turmeric (Curcuma) resulted in the secondary metabolite, curcumin (**1**) as the major component (Fig. 1.). Besides curcumin, there are also natural curcuminoids present in turmeric like demethoxy or partly saturated curcumin derivatives. Several clinical trials have been conducted in cancer, cardiovascular diseases, diabetes, inflammatory diseases, toxicology, etc. to evaluate their pharmacological behaviors (Gupta, et al., 2013). Extensive worldwide research has shown that, due to its pleiotropic character, curcumin's pharmacological effects are extremely diverse and have many molecular targets with multiple biochemical pathways as a cytotoxic antiproliferative agent (Oliveira et al., 2015; Aggarwal et al., 2003). In the structure of curcumin, 1,7-bis (4-hydroxy-3-methoxyphenyl)-1,6-heptadien-3,5-dione, there are seven carbon atoms between the two aromatic rings (Fig. 1.).

This C_7-linkage is a 1,6-heptadien-3,5-dione moiety in the C_7-curcumin molecule. This triviality is important since the C_5-curcumin (**2**), 1,5-bis(4-hydroxy-3-methoxyphenyl)-1,4-pentadiene-3-one (Fig. 1.),

* Corresponding author: Department of Pharmaceutical Chemistry, University of Pécs, H-7624 Pécs Rokus str 2, Hungary.
E-mail address: imre.huber@aok.pte.hu (I. Huber).

https://doi.org/10.1016/j.ejps.2022.106184
Received 20 January 2022; Received in revised form 26 March 2022; Accepted 4 April 2022
Available online 10 April 2022

was discovered in 1993 (Masuda et al., 1993). The truncated curcumin **2** bears a C_5 β-dienone linker (1,4-pentadiene-3-one) and was isolated along with C_7-curcumin from different *Curcuma* species (Masuda et al., 1993). The term "C_5-curcumin" was used in a publication describing structure-activity relationship (SAR) analysis among such compounds (Kohyama et al., 2015). These synthetic C_5-curcuminoids have shown superior cytotoxicity and a much better pharmacokinetic profile due to higher structural stability compared to curcumin (Liang et al., 2009). Whether C_5-curcumin is a metabolite of C_7-curcumin or not, the truncated monocarbonyl curcumin (**2**) can be synthesized from the dicarbonyl curcumin (**1**) in a pyrolysis reaction (Dahmke et al., 2014). The reaction was carried out in coconut oil, suggesting that people eating meals containing turmeric from the wok are consuming C_5-curcumin (**2**) in a considerable amount per year. It was also proved, that the pyrolysis product "deketene curcumin" (**2**) has a five-fold higher gastric tumor growth-inhibiting activity compared to C_7-curcumin (**1**) in an *in vivo* mouse model (Yoshida et al., 2018).

A special subgroup of the C_5-curcuminoids is the so-called cyclic C_5-curcuminoids. There are a couple of recent review articles about the chemistry, pharmacology, biological activity, physicochemical characteristics and mechanism of action of such derivatives of this subgroup (Oliveira et al., 2015, Das et al., 2009, Huber, 2020). There are more than 300 valuable references in these reviews reflecting the most important research results about curcumins and cyclic C_5-curcuminoids. Members of this subgroup contain a central ring in their structure. This ring is carbocyclic or heterocyclic, usually cyclopentanone, cyclohexanone, 4-hydroxycyclohexanone, 4-piperidone, 4-pyranone, holding two benzylidene groups both adjacent to the ketone carbonyl function. Such examples are compound **5** with cyclohexanone, CLEFMA, EF24 (**3**) or compound **7** with 4-piperidone and VLX1570 with 4-azepinone ring as indicated in Figs. 1. and 3. The introduction of the ring into the cross-conjugated β-dienone spacer of these cyclic C_5-curcuminoid compounds constrains the structure into a "close-to-planar" 3D shape as depicted in Fig. 2., with the conformational movements kept on the minimum compared to C_5-curcumin or C_7-curcumin. The atoms of the central cyclanone ring together with the olefinic CH groups are practically located in one plane except position 4, opposite to the ketone carbonyl function (Lotfy et al., 2019). The free rotation of the aromatic rings is hindered, especially when they bear at least one *ortho* substituent. In general, cyclic C_5-curcuminoid derivatives with a relatively

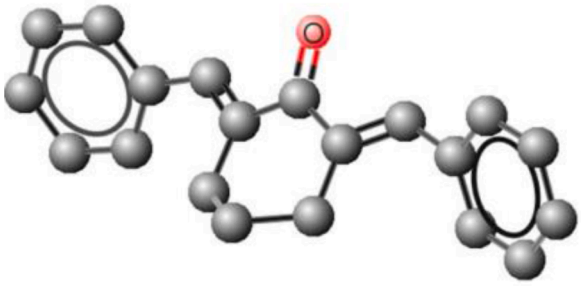

Fig. 2. Cyclic C_5-curcuminoid, 2,6-dibenzylidene-cyclohexanone, in a "close-to-planar" structure with restricted conformational flexibility. Generated by ChemAxon's Marvin Suite (ChemAxon, 2022). Supported also by X-ray data (Lotfy et al., 2019).

rigid structure show reduced conformational activity that appears to be important to increase their pharmacological activity compared to C_7-curcumin itself.

Curcumins and cyclic C_5-curcuminoids were subjected to several SAR studies (Oliveira et al., 2015; Kohyama et al., 2015; Das et al., 2009, Jiang et al., 2012; Kohyama et al., 2016; Mapoung et al., 2019; Das et al., 2013; Santiago-Vazquez et al., 2014). These research works aimed to find the most important structural modifications necessary to obtain the best cytotoxic effect. In addition to much higher anticancer activity, cyclic C_5-curcuminoids have shown also superior stability compared to curcumin in terms of their less susceptibility to hydrolysis and metabolism; see, for example (Zhang et al., 2018) and (Liu et al., 2018). Another positive characteristic is their excellent tolerability in mammals, see, for example (Yuan et al., 2014) and (Anchoori et al., 2013) in this respect.

Figs. 1. and 3. describe some important examples representing the advances in the research of cyclic C_5-curcuminoids in particular, their antiproliferative activity. 4-[3,5-Bis(2-chlorobenzylidene)-4-oxo-piperidine-1-yl]-4-oxo-2-butenoic acid (CLEFMA, Fig. 1.) as a synthetic C_5-curcuminoid possesses anti-inflammatory, and anticancer properties against osteosarcoma (Yang et al., 2019) and H441 lung adenocarcinoma cells (Sahoo et al., 2012). A common property of VLX1570 (Fig. 1.) and related derivatives is their targeting of the ubiquitin-proteasome system (UPS), known to be essential for the viability of different

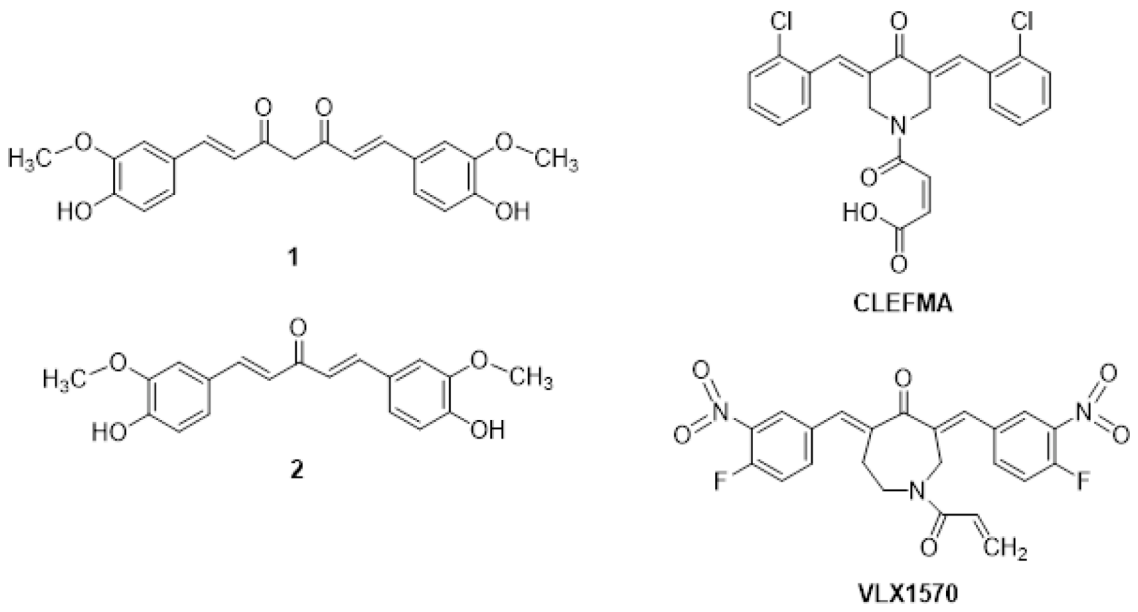

Fig. 1. C_7-curcumin (**1**) and C_5-curcumin (**2**), both of them natural, isolated from *Curcuma longa L.* and *Curcuma domestica L.*. Cyclic C_5-curcuminoids CLEFMA and VLX1570 are synthetic antiproliferative drug candidates.

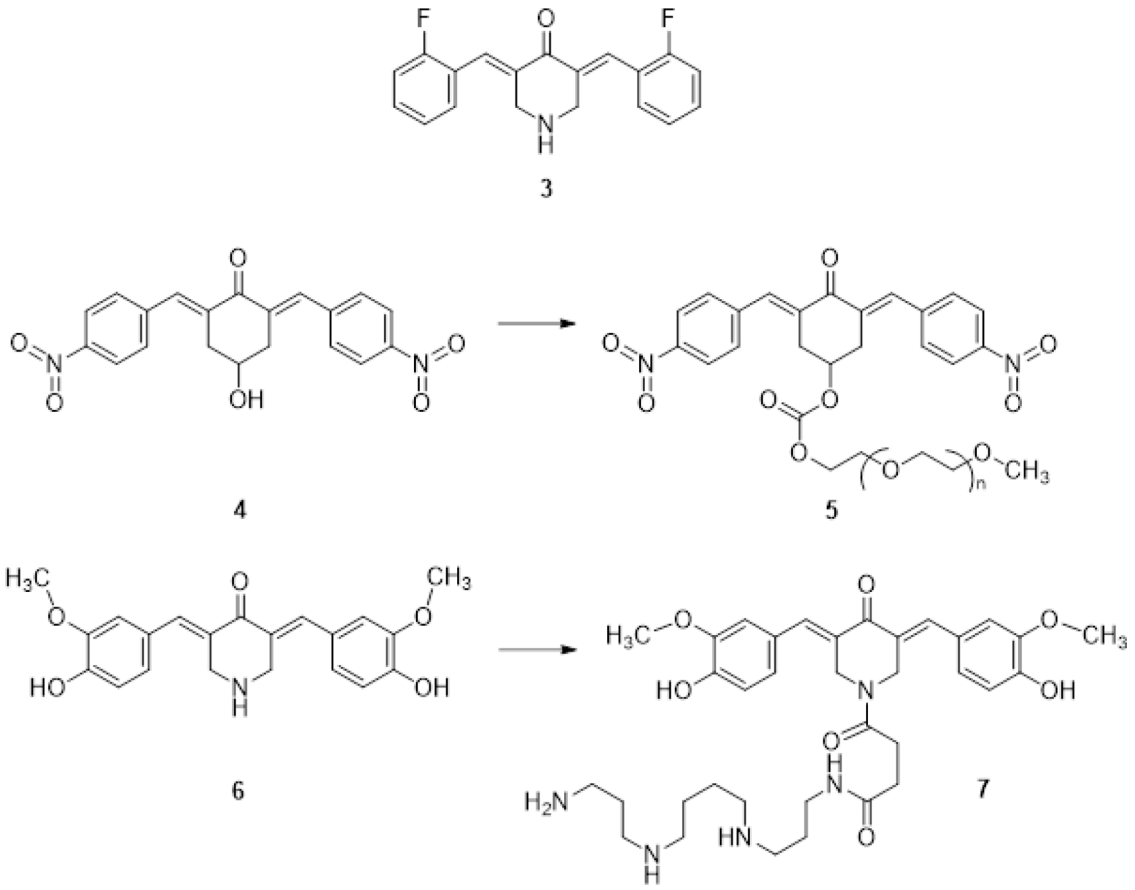

Fig. 3. Cyclic C_5-curcuminoid EF24 (**3**), PEGylated ester (**5**) and spermine (**7**) derivatives.

cancer cells. Preclinical studies of VLX1570 together with other promising compounds in multiple myeloma are reviewed in two recent papers (Innao et al., 2021; Bazzaro and Linder, 2020). The antitumor pharmacology of EF24 (**3**, Fig. 3.) has been proven in studies on hepatocellular carcinoma, adrenocortical tumors, colorectal cancer, cholangiocellular carcinoma, oral squamous cell carcinoma and pancreatic cancer (Bazzaro and Linder, 2020).

EF24 (**3**) molecule is one of those rare cyclic C_5-curcuminoids which has shown cytotoxic activity in human neuroblastoma (SH-SY5Y cells) in combination with irradiation and mitigation of the survival of cancer cells (Aravindan et al., 2013). Spermine derivatives like polyamine conjugated compound **7** (Fig. 3.) were also tested on human neuroblastoma (SH-SY5Y) model (Simoni et al., 2010). The authors disclose that the polyamine motif in compound **7** decreases the cytotoxic strength of the heterocyclic C_5-curcuminoid **6**, however, it works as a promising tool in targeted drug delivery of the polyamine transport system mediated cell import processes. Studies on neuroprotective natural C_7-curcuminoids are also available in the corresponding literature, see, for example (Mufti et al., 2015).

A comparative SAR study was conducted on cyclic C_5-curcuminoids involving their activity on glioblastoma (U87MG) cells (Cersosimo et al., 2015). One of the best performers was derivative **4** (Fig. 3.) with an IC_{50} value of 4.62 μM. This derivative has been selected for "PEGylation" reaction to form the "PEGylated" congener **5** (Fig. 3.). The PEGylated compound bears a polyethylene glycol type substituent providing a tool for liposomal prodrug formulation. Compound **5**, being Michael acceptor, proved to be a highly active isopeptidase (a cellular thiol type cysteine-protease) inhibitor. A review article on studies of natural C_7-curcuminoids on glioblastoma is also available in the corresponding literature (Shabaninejad et al., 2020).

Neuroblastomas are the most common malignant solid tumors of the nervous system occurring in childhood. Gliomas are the most common primary tumors of the central nervous system (CNS) manifesting in astrocytes or glial cells of the brain. A limited number of publications is available about cyclic C_5-curcuminoids tested on neuroblastoma and glioblastoma (glioblastoma multiforme) or its more aggressive form, IV grade astrocytoma. Therefore, we have decided to synthetize novel derivatives **8-13, 17** and **19-22** of this subgroup of curcuminoids aiming to test their effect on the viability of SH-SY5Y, human neuroblastoma and of the CCF-STTG1, human grade IV astrocytoma cell lines. Our purpose was also to investigate their ability to penetrate the blood-brain barrier and to analyze their SAR behaviors.

2. Results and discussion

2.1. Design and synthesis

One of the major interests in our laboratories is the design, synthesis and antineoplastic evaluation of cross-conjugated cyclic C_5-curcuminoids. During design and syntheses hydrogen or halogen *p*-substitution on the benzylidene rings was favored instead of alkyl or alkoxy due to our earlier findings where this seemed to be beneficial on cytotoxicity (Huber et al., 2015; Huber et al., 2019, 2020). As a continuation of our former studies in this field we have prepared compounds **8-13** (Fig. 4.), **17a-e** (Scheme 1.), **19a-b, 20, 21** (Scheme 2.) and **22** (Scheme 3.) for further biological testing. Pyridinyl derivatives **8** and **9** were synthesized according to our previous publication (Huber et al., 2019) from 4-hydroxycyclohexanone and the corresponding pyridincarbaldehyde under the conditions of the *Claisen-Schmidt* condensation reaction. Heterocyclic derivatives **10** (Huber et al., 2019) and **11-13** were prepared following our modified "one-pot" *Claisen-Schmidt* condensation (Huber et al., 2015). Compounds **8-12** were selected to be tested due to

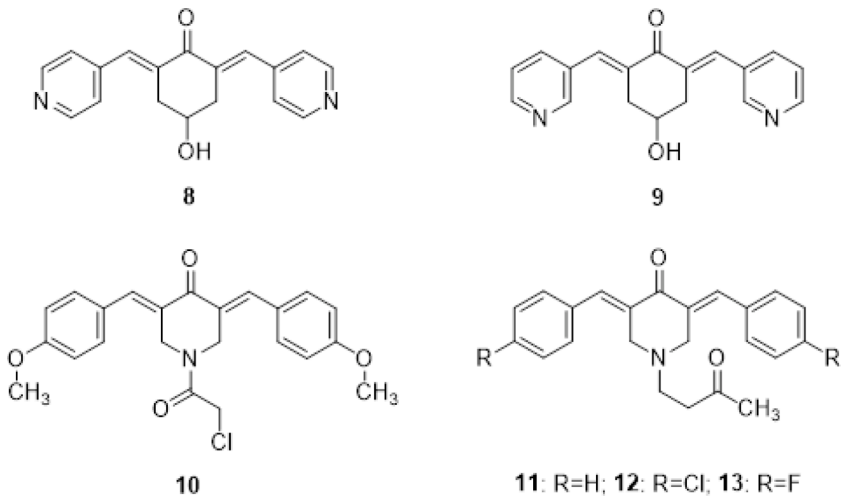

Fig. 4. Cyclic C_5-curcuminoid derivatives **8-13** with documented IC_{50} values in the low- or submicromolar range against different solid tumor cells were produced according to our previously described methods (Huber et al., 2015; 2019; 2020).

their very good performance on our earlier viability studies against different human cancer cell lines. For instance, 2,6-bis[(4'-pyridinyl) methylene]-4-hydroxycyclohexanone (**8**) is active in IC_{50} = 0.76 μM (A2780 ovarian), 2.69 μM (C33A cervix) and 1.28 μM (MDA-MB-231 breast) concentrations, or compound **10** in IC_{50} = 1.34 μM (A2780), 1.51 μM (C33A), 1.00 μM (MDA-MB-231) (Huber et al., 2019). The N-alkyl derivatives **11** and **12** have shown their IC_{50} values against four human adherent cancer cell lines like HeLa, A431, A2780 and MCF7 even in the submicromolar range (Huber et al., 2015). Compounds **8-12** served as internal standards of this investigation with their activity compared to that of reference drug Cisplatin (Huber et al., 2015; 2019).

Local anesthetics, like lidocaine, are well-known drugs in pharmaceutical chemistry about their ability to penetrate into neurons (Watson, 2011). This ability is due to the presence of the protonation-deprotonation equilibrium of weakly basic nitrogen in their structure. The presence of weakly basic nitrogen and structural similarity between lidocaine and compounds **17** is obvious (Scheme 1.). These compounds (**17a-j**) were designed and prepared on this base for testing on neuroblastoma and astrocytoma cancer cell lines of the present study. According to the classical synthesis of lidocaine, appropriately substituted anilines **14** were acylated with chloroacetyl chloride followed by the N-alkylation of 4-piperidone with intermediates **15** in the presence of triethylamine. Compounds **16** were then used as starting materials for the base-catalyzed *Claisen-Schmidt* condensation reactions with different aromatic benzaldehydes to obtain the targeted compounds (**17a-j**) for further biological testing. It is worthy of note, that, owing to the weak basicity of the nitrogen atom in **18** coupled with the low alkylating strength of **15**, the desired compounds **17** could not be prepared if started from compounds **18** under mild conditions used by us (Scheme 1.).

Another major interest in our laboratories is the research on biological barriers. The function of monocarboxylic acid transporters in the CNS targeted active drug transport through the blood-brain barrier (BBB) is well established about the model used in this study (Veszelka et al., 2018; Bors and Erdő, 2019). Our goal was, therefore, to synthesize cyclic C_5-curcuminoids **19** and **21** (Scheme 2.) in order to gain information on their possible function, such as delivery across the BBB. To our best knowledge, this is the first attempt among cyclic C_5-curcuminoids in this respect. The starting materials **18a-c** (Schemes 2. and 3.) used for the synthesis of target compounds **19-22** were prepared according to our previously described "one-pot" method (Huber et al., 2015). For the acylation reactions of compounds **18a-c** acid anhydrides or acid chlorides were used to obtain the desired derivatives **19, 21** and **20, 22** respectively.

The N-substituents of the 4-piperidone ring in the structure of compounds **19-22** (Schemes 2. and 3.) can be a promising tool in CNS delivery of these potential prodrugs.

Structures of the compounds synthesized were established utilizing ^1H, ^{13}C NMR and MS spectroscopic measurements. The *E,E*-configuration of the newly synthesized compounds was determined by ^1H NMR (Huber et al., 2019). The *E,E*-configuration is due to the anisotropic effect of the adjacent cyclic carbonyl group on the vinyl protons, which is not possible in the *Z,Z*-configurational forms. In some instances (like compound **19a, 19b, 20**) the doubling of the aromatic and some olefinic ^{13}C signals was observed. It is in accordance with the proposed (Lotfy et al., 2019) rigid "close-to-planar" nature of the cyclanone ring system (Fig. 2.) when certain structural criteria, like the presence of a suitable torsion angle between the planes of the two aromatic rings are fulfilled. MS analysis: we have investigated several analytes in the series of 3, 5-dibenzylidene-4-piperidones and other 2,6-dibenzylidene-1-cyclanones. In general, we can state that the diagnostic product ions were not only fragments but also dimers or sometimes trimers of the molecular ions in their MS spectra. The unexpected dimerization, together with $[M+H]^+$ ion formation in positive mode is a typical MS character of our new compounds following our earlier findings (Huber et al., 2019).

2.2. Cytotoxicity and SAR

We tested the cytotoxic effects of the synthetized cyclic C_5-curcuminoids **8-13, 17** and **19-22** on neuroblastoma and astrocytoma cells to determine the effectiveness of the active agents against CNS tumors. Compounds **8-12** served as internal standards of this investigation with their activity compared to that of reference drug Cisplatin (Huber et al., 2015, 2019). According to the literature these cells are widely used for cytotoxicity measurements as the model of the cells of the CNS (Dalberto et al., 2020; Wang et al., 2015; Romero et al., 2017; Leone et al., 2015). Based on the data obtained from these experiments, SH-SY5Y and CCF-STTG1 cells are quite resistant to harmful substances, the cytotoxic agents were used usually in μM concentration (Dalberto et al., 2020; Raszewski et al., 2015, 2016, Woehrling et al., 2006; Krug et al., 2018). Interestingly, the toxic effect of curcuminoids **8-13, 17** and **19-22** on the cells did not show an exponential increase suggesting that the relatively low concentration of the compounds (0.1 nM - 10 nM) had reached their maximum effect by binding to their multiple targets (Das et al., 2009) mainly bio thiols in the cells at 48 h. One example of such cellular thiols are the isopeptidases, member of the cysteine-protease family of enzymes, responsible for triggering necrosis and/or apoptosis (Cersosimo et al., 2015). The viability values showed that the curcuminoids **8-13,**

17 and **19-22** were more effective on astrocytoma compared to neuroblastoma except for **19b** and **21**, which exerted three times greater effects on neuroblastoma cells (Table 1.). Derivatives **11, 12, 19a, 19b** and **21** presented the lowest IC_{50} values, less than 1 nM. The most powerful effect was found using **11** on astrocytoma cells (IC_{50} 0.26 nM) and **19b** on neuroblastoma cells (IC_{50} 0.14 nM). In the case of the less effective curcuminoid **17c** we calculated 7.48 and 5.65 IC_{50} values on neuroblastoma and astrocytoma cells, respectively (Table 1.). Compounds **17f-j** did not show cytotoxicity in concentrations used (0.1 nM - 10 nM) for 48 h for viability tests.

Although the examined compounds were successful in decreasing the viability of the tumor cells, the determination of toxicity on healthy cells could not be avoided. We chose C8-D1A astrocytes as a healthy *in vitro* model of CNS glial cells (Khan et al., 2018; Tantarungsee et al., 2018). To reveal the possible systemic effect of the curcuminoids, the Cos-1 kidney cells were used as model (Govindaraju et al., 2018; Dubuc et al., 2019; Choedon et al., 2006). The case of the treatments with **11, 17d, 19b** and **20** astrocyte cells showed higher viability compared to both neuroblastoma and astrocytoma cells proposing that these active compounds were less toxic to normal astrocytes. In addition, C8-D1A astrocytes were also less sensitive to **12, 13, 17b, 17c** and **17e, 19a, 22** compared to the astrocytoma cell line. Furthermore, **19b** and **21** were less toxic to astrocytes compared to SH-SY5Y cells. The remaining four curcuminoids, **8, 9, 10** and **17a** were more harmful to the astrocytes than to the tumorous cells. The same four compounds together with**19a** and **22** were toxic to the Cos-1 kidney cells as well. On the other hand, we found that seven curcuminoids (**12, 13, 17b, 17c, 17d, 17e** and **20**) were less toxic to kidney cells compared to the astrocytoma cells and treatments with two active compounds (**19b** and **21**) resulted in higher cell viability of Cos-1 cells, as well. Interestingly, only **11** was less effective on the cell viability of kidney cells compared to both tumorous cell lines (Table 1.). The highest selectivity was shown in case of compound **11** (5.50 to astrocytes), **17d** (4.95 to astrocytes) and **19b** (6.17 to kidney cells) suggesting that these curcuminoids are very effective against CNS tumorous cell lines and some of them less toxic toward healthy cells. Selectivity was also observed when none of the tested curcuminoids **12, 17c** and **19b** caused cell toxicity on primary rat brain endothelial cells used for BBB permeation model (see details later and Fig. S2.).

Concerning SAR, we found the following facts noteworthy. Among the 21 derivatives tested, compounds showed different antiproliferative activity rate in rising order of **17a-j** (IC_{50} = 1.44-7.48, average 4.89 nM), N-(ɣ-oxobutyl)-substituted compounds **11-13** (IC_{50} = 0.26-2.14, average 0.90 nM) and monocarboxylic acid derivatives **19-21** (IC_{50} = 0.14-1.19, average 0.53 nM) (Table 1.). The *p*-trifluoromethyl substituent on the benzylidene rings dominates the *p*-chloro- or *p*-methoxy-, like in the case of compounds **17e, 17i** and **17h**, or in case of **17b** and **17c**. *p*-Chloro- substitution of **17d** provided a more active derivative compared to the corresponding *p*-methoxy- counterpart **17g**. No activity could be exploited among the lidocaine analog **17** counterparts with *p*-methoxy-benzylidene (**17f-h**) or 2',4'-dichloroanilinyl (**17h-j**) substituents in the concentration range used (0.1 nM - 10 nM) by us. In the subgroup of N-(ɣ-oxobutyl)-substituted compounds **11-13** the only structural difference is the *p*-substituent of the benzylidene ring: hydrogen atom in **11**, chlorine atom in **12** and fluorine in **13**. The increasing order of activity on both cancer cell lines was **11**>**12**>**13**. The highest anti-cancer activity was observed among substances substituted with an N-monocarboxylic function (**19-21**). The open-chain butyric acid derivatives (**19a, 19b**) proved to be more potent compared to the correspondingly substituted cyclohex-3-enyl (**20**) or esterified

Table 1
Calculated IC_{50} (nM) values on the different cancer and non-cancer cell lines were found in the low nanomolar or picomolar range. Selectivity indices are calculated from the corresponding IC_{50} data (non-cancer value divided by the cancer one). Compounds **17f-j** did not show cytotoxicity in concentrations used (0.1 nM–10 nM) for 48 h for viability tests. Cisplatin was used as positive control.

Compound	Neuroblastoma (SH-SY5Y)	Astrocytoma (CCF-STTG1)	Kidney cells (Cos-1)	Healthy astrocytes(C8-D1A)	Selectivity Index(Neuroblastoma and Astrocytoma)
8	3.46 (±0.10)	2.45 (±0.21)	0.12 (±0.03)	1.62 (±0.20)	0.03/0.47 and 0.05/0.66
9	4.03 (±0.13)	1.86 (±0.19)	1.74 (±0.17)	1.61 (±0.10)	0.43/0.40 and 0.93/0.86
10	6.33 (±0.21)	3.74 (±0.28)	1.58 (±0.14)	3.44 (±0.29)	0.25/0.54 and 0.42/0.92
11	0.82 (±0.19)	0.26 (±0.13)	0.82 (±0.10)	1.41 (±0.10)	1.00/1.72 and 3.20/5.50
12	0.99 (±0.25)	0.51 (±0.09)	0.87 (±0.18)	0.85 (±0.10)	0.88/0.85 and 1.70/1.65
13	2.14 (±0.07)	0.68 (±0.14)	0.84 (±0.11)	0.93 (±0.14)	0.40/0.43 and 1.24/1.36
17a	5.48 (±0.30)	3.60 (±0.33)	1.68 (±0.0.22)	1.85 (±0.14)	0.31/0.34 and 0.47/0.51
17b	5.48 (±0.22)	1.44 (±0.09)	1.63 (±0.19)	3.16 (±0.17)	0.30/0.58 and 1.13/2.19
17c	7.48 (±0.32)	5.65 (±0.41)	6.93 (±0.41)	6.92 (±0.50)	0.93/0.93 and 1.23/1.23
17d	7.35 (±0.45)	2.65 (±0.20)	4.58 (±0.23)	13.12 (±0.54)	0.62/1.79 and 1.73/4.95
17e	5.92 (±0.29)	3.86 (±0.32)	4.90 (±0.28)	3.90 (±0.27)	0.83/0.66 and 1.27/1.01
19a	0.94 (±0.13)	0.49 (±0.04)	0.19 (±0.05)	0.91 (±0.11)	0.12/0.97 and 0.38/1.85
19b	0.14 (±0.04)	0.39 (±0.09)	0.18 (±0.03)	0.86 (±0.13)	1.26/6.17 and 0.45/2.21
20	1.19 (±0.07)	0.50 (±0.10)	0.80 (±0.10)	1.41 (±0.12)	0.67/1.19 and 1.60/2.82
21	0.15 (±0.05)	0.42 (±0.07)	0.15 (±0.03)	0.27 (±0.07)	1.06/1.86 and 0.37/0.64
22	4.19 (±0.40)	3.06 (±0.14)	0.10 (±0.03)	3.46 (±0.17)	0.02/0.83 and 0.03/1.13
Cisplatin	19.94 (±1.11)	7.07 (±0.59)	9.17 (±0.84)	7.77 (±0.89)	0.46/0.39 and 1.30/1.10

(**21**) counterparts. The *p*-trifluoromethyl-benzylidene substitution in compound **19b** showed superior activity over *p*-chlorobenzylidene **19a**. The outcome of the present cytotoxicity tests confirms our earlier finding that the presence of halogen atom(s) in the *p*-position of the benzylidene rings increases the cytotoxic activity compared to alkyl or alkyloxy (Huber et al., 2015, 2019, 2020). It is described about enones and dienones like chalcones and curcuminoids, that their unique biochemical reaction is the selective thia-Michael reaction which is reversable, leading to equilibrium (Huber, 2020). The thia-Michael acceptor character and the strength/weakness of the carbon-sulphur bond formed in this reaction is directly correlated with the electrophilicity of the dienone system. The presence of the halogen atom(s) in the *p*-position of the benzylidene rings increases the reactivity of these cyclic C_5-curcuminoids in the Michael reaction toward the -SH functional groups of bio thiols in the cells. Regardless of the type of the structure, the highest selectivity was found in cases **19b, 11** and **17d**, respectively (Table 1.).

2.3. Lipophilicity, experimental logP and calculated dipole moment

Based on previous results (Huber et al., 2020) we measured the log*P* values of the synthesized and tested cyclic C_5-curcuminoid compounds **8-13, 17** and **19-22.** The method we worked out and used is a chromatographic measurement in a reversed-phase thin-layer chromatographic (RP-TLC) setting. The theoretical background of it is a relation between the partition coefficient and the retention factor (R_M for RP-TLC) based on liquid/liquid partition. R_M values (calculated using R_f) are in a linear correlation with log*P* values in a suitable chromatographic system according to the

$$\log P = aR_M + b$$

equation. See experimental for details.

Results from the RP-TLC measurements for experimental $\log P_{TLC}$ data are summarized in Table 2. together with the corresponding IC_{50} values and some calculated physicochemical parameters.

To visualize the relationship between experimental $\log P_{TLC}$ and IC_{50} data we have plotted them against each other. The diagrams on the two cancer cell lines are in Fig. 5. Our goal was to determine if there was a correlation between the obtained log*P* data and the pharmacological activity of model compounds **8-13, 17a-e, 19a,b, 20-22**. To have deeper insight, the data from Table 2. underwent calculations according to Pearson correlation and Kendall coefficient of concordance. There was

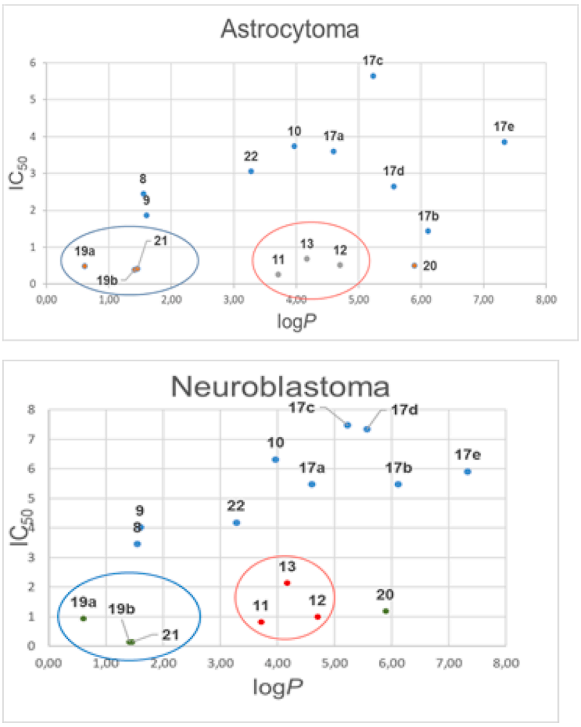

Fig. 5. Relationship between antiproliferative activity against astrocytoma or neuroblastoma cancer cell lines and lipophilicity of compounds **8-13, 17a-e, 19a,b** and **20-22**. Experimental $\log P_{TLC}$ and IC_{50} (in nM) values were plotted against each other. The best performers on both cell lines are N-monocarboxylic acid derivatives **19a, 19b** and **21** in blue, and N-oxobutyl compounds **11-13** in red ellipses.

no consistent relationship that could be established between antiproliferative activity and lipophilicity of our model compounds in this study (see for example Supplementary material, Table S1.). The lack of a strong positive or negative correlation does not mean, however, that there is no correlation between the nature of the structure and the biological activity at all. The most promising compounds **8-9** or **19a, 19b** and **21** for example, have their log*P* value under 2 due to a possible increase of water-solubility protonation (**8-9**) or acid anion formation (**19, 21**) at physiological pH. Good performing compounds, like **11-13**

Table 2
IC_{50}, experimental $\log P_{TLC}$ and Clog*P*, Clog*D*, calculated dipole moment (Debye), 2D polar surface area (PSA 2D), water solubility and protonation values at physiological pH. ChemAxon's Marvin Suite (ChemAxon, 2022) was used for calculations.

Comp.	Neurobl.IC_{50} (nM)	Astrocyt. IC_{50} (nM)	Exp. $\log P_{TLC}$	Clog*P*	Clog*D*	Dipole Moment	PSA 2D	Solubilityin water (mg/L)	Protonation (%)
8	3.46	2.45	1.55	1.23	1.22	1.86	66.32	1336.24	0.96
9	4.03	1.86	1.60	1.23	1.22	1.71	66.32	1336.24	0.53
10	6.33	3.74	3.97	4.14	4.14	2.86	55.84	0.94	0
11	0.82	0.26	3.71	5.03	5.02	3.96	37.38	6.43	0.50
12	0.99	0.51	4.70	6.06	6.06	3.97	37.38	0.34	0.32
13	2.14	0.68	4.17	5.30	5.30	3.88	37.38	2.36	0.27
17a	5.48	3.60	4.60	5.84	5.84	3.17	49.41	0.25	0.04
17b	5.48	1.44	6.11	7.60	7.60	3.86	49.41	0.006	0.02
17c	7.48	5.65	5.23	6.87	6.87	2.74	49.41	0.02	0.02
17d	7.35	2.65	5.56	7.81	7.81	4.36	49.41	0.006	0.02
17e	5.92	3.86	7.33	8.64	8.64	2.49	49.41	0.0006	0
19a	0.94	0.49	0.61*	4.89	1.65	2.57	74.68	337.04	acid anion**
19b	0.14	0.39	1.41*	5.62	2.38	1.53	74.68	161.73	acid anion**
20	1.19	0.50	5.89	6.83	6.83	3.33	63.68	0.02	0
21	0.15	0.42	1.46*	6.77	3.58	3.04	74.68	22.43	acid anion**
22	4.19	3.06	3.28	4.48	4.48	2.30	50.27	0.51	0.02

* These values are out of the range of the method used. Samples of these polar compounds did not move on the TLC plate with the developing mixture. **100% deprotonated.

or **17b,d** (astrocytoma) however, have higher log*P* even above 6. The practically ineffective lidocaine analogs **17f-j** (Table 1.) have their log*P* in the range of 4.93-6.64 (4.93; 5.15; 6.37; 6.64 and 6.11 respectively), but compound **17e** with a moderate anticancer activity has a 7.33 log*P* value. So, the log*P* value alone will not determine the efficacy of the cyclic C_5-curcuminoids investigated here in good accordance with our earlier findings (Huber et al., 2020).

We performed an analysis using the calculated dipole moment values (Table 2.) with very similar results (Supplementary material, Fig. S1.). Sufficient correlation was found between experimental logP_{TLC} and Clog*P* or Clog*D* data (Table 2.). See the correlation between logP_{TLC} and Clog*D* data in Supplementary material, Fig. S5.

Solubility in water and cytotoxic activity (IC_{50}) of the compounds (Table 2.) compared to each other comprises contradictions. First of all, not only compounds with elevated water-solubility showed remarkable decrease in viability of tumorous cells. For example, derivatives **19a** (IC_{50} = 0.49 nM) and **12** (IC_{50} = 0.51 nM) have similar activity on astrocytoma cells with different calculated solubility: 337 mg/L for **19a** and 0.34 mg/L for **12**. Likewise, compounds **8** (IC_{50} = 2.45 nM) and **17e** (IC_{50} = 3.86 nM) on astrocytoma with 1336 mg/L and 0.0006 mg/L solubility, respectively. On neuroblastoma cells compounds **11** (IC_{50} = 0.82 nM) and **20** (IC_{50} = 1.19 nM) with 6.43 mg/L and 0.02 mg/L calculated solubility. To solve this contradiction, beside possible metabolism, there is another explanation, namely the addition of the cellular thiols over the Michael acceptor ß-dienone function of the compounds has a solubility increasing influence of cyclic C_5-curcuminoids (Huber, 2020). The high cytotoxic activity combined with a very low solubility in water (like **12, 17e** and others in Table 2.) provides secondary evidence on the solubility increasing effect of the thia-Michael reaction.

Based on the results of the cytotoxicity tests on the two cancer cell lines and on logP_{TLC} – calculated physicochemical data/IC_{50} correlations and SAR analysis we have identified three subgroups of the compounds tested. One of these three was subgroup **17a-j** with the lowest average antiproliferative activity. The second group in this order is represented by compounds **8-10** and **22** with higher anticancer effects. The most promising subgroup comprises derivatives **11-13, 19** and **21** with the lowest IC_{50} and log*P* data. We selected one N-monocarbaxylic acid (**19b**), one N-oxobutyl (**12**) derivatives from the most active subgroup and the lidocaine analog compound **17c** from the less active subgroup, to test their ability to permeate the blood-brain barrier (BBB).

2.4. Effect of cyclic C_5-curcuminoid derivatives 12, 17c and 19b on cell viability of rat brain endothelial cells and permeation through the BBB

Perhaps the most important novelty of the synthesized compounds is described here. This is the first example describing BBB permeating cyclic C_5-curcuminoids in the corresponding literature to our best knowledge. First of all, we measured the toxicity of the selected three compounds on the cells in a well characterized BBB culture model. None of the tested curcuminoids **12, 17c** and **19b** caused cell toxicity on primary rat brain endothelial cells up to 100 nM concentration for 24 h (Supplementary material, Fig. S2.). All curcuminoid concentrations run similarly to the control group (red) except the highest, 100 nM concentration of **12**, which increased impedance. To verify that this result is due to the effect of **12** itself, we retested this concentration in a repeated experiment.

We increased the concentration range to see at which concentration the tested curcuminoids cause cell damage. The tested curcuminoids **12, 17c** or **19b** caused no cell toxicity on primary rat brain endothelial cells at 10 μM and lower concentrations for 48 h (Fig. 6.). All curcuminoid concentrations run similarly to the control group (red) except the highest, 30 μM concentrations, which decreased impedance indicating a damaging effect to the barrier. In accordance with the former results (Supplementary material, Fig. S2.), compound **12** elevated the impedance of brain endothelial cells, indicating a possibly beneficial effect on the barrier (Fig. 6.).

Based on the results of experiments prior to the BBB permeability tests, we selected the 1 μM concentration as optimal for all three molecules.

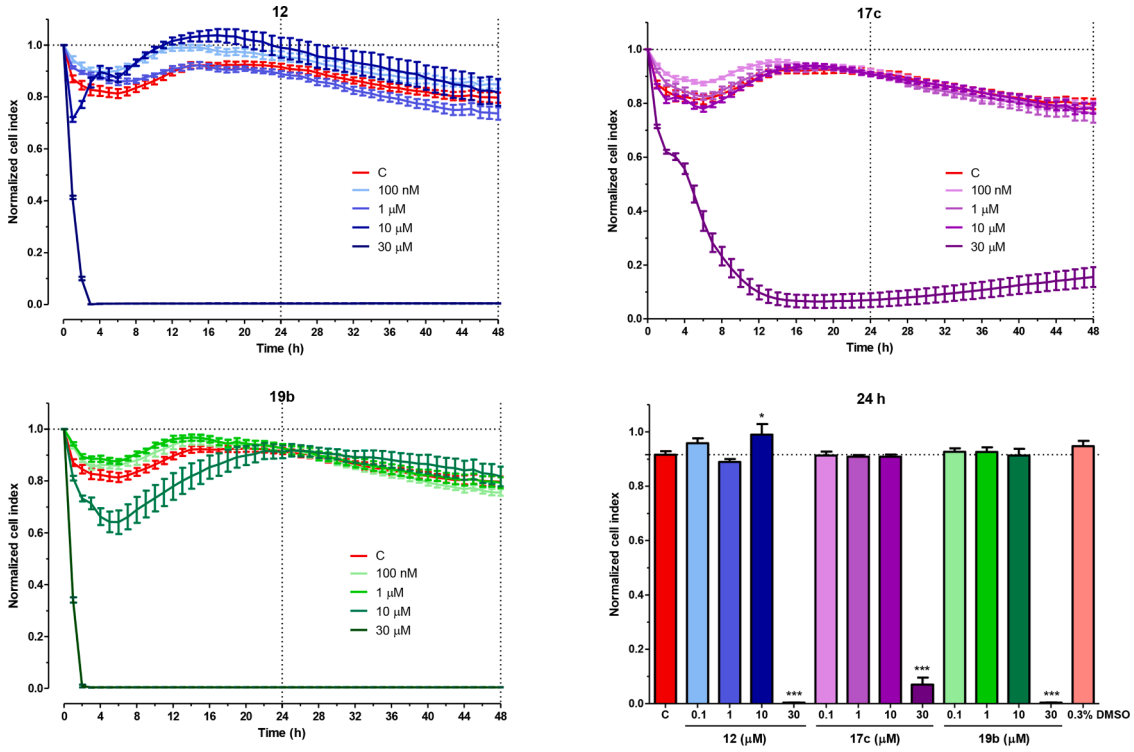

Fig. 6. Kinetics of the effect of different concentrations of **12,17c, 19b** and 0.3% DMSO, the solvent of the compounds on the impedance of rat brain endothelial monolayers. Mean ± SD, n = 6-8, ANOVA, Bonferroni test, *p < 0.05, ***p < 0.001 compared to the control group.

During the culture of the BBB model increasing transendothelial electrical resistance (TEER) values were registered. On the 4th day of co-culture, high TEER values were measured (450 Ω × cm^2) indicating the tightness of the barrier. This tightness was mirrored in the low permeability values (Fig. 7.). The BBB model showed a very low permeability for the water-soluble markers fluorescein (**5.55 × 10^{-7} cm/s**) and Evans blue-albumin complex (**0.37 × 10^{-7} cm/s**), indicating good tightness of the model for permeability studies (Helms et al., 2016).

As a result of the permeability tests, we can state, that two of the three compounds had a higher penetration across the BBB model, than the passive permeability markers. Both **17c** (**24.48 × 10^{-7} cm/s**) and **19b** (**11.65 × 10^{-7} cm/s**) had higher penetration across the BBB model compared to the marker molecules (Fig. 7.), while the penetration of **12** (**3.01 × 10^{-7} cm/s**) was in the range of that of the passive small hydrophilic marker, sodium fluorescein (Fig. 7.). In our previous studies using the same BBB model (Veszelka et al., 2018; Nakagawa et al., 2009; Hellinger et al., 2012) we measured a wide range of drugs with different levels of CNS penetration. As a comparison, the BBB penetration of the drugs gabapentin used in the treatment of epilepsy and neuropathic pain (Veszelka et al., 2018) or the cytostatic vinblastine (Nakagawa et al., 2009; Hellinger et al., 2012) were in the range of that of **17c** and **19b**. In contrast, the permeability of **12** was similar to digoxin (Nakagawa et al., 2009), which is known not to enter the CNS in healthy conditions. **17c** showed significantly higher P_{app} values than **12** and **19b**. The penetration of **19b** was significantly increased compared to **12** (Fig. 7.) what can be the result of the presence of monocarboxylic acid transporters in cells of the BBB model, that may help the transfer of **19b**, a monocarboxylic acid derivative across the BBB model (Veszelka et al., 2018).

The dissimilarity in the permeability values seen in Fig. 7. can be explained, besides the differences in structure and log*P* values, with different binding abilities to bovine serum albumin (BSA) of the compounds tested. BSA was used as a physiological solubilizer and oncotic molecule throughout these experiments. We focused on BSA-binding when the mass balance of curcuminoids was determined. The recovery (mass balance) of the three tested derivatives was very different (Supplementary material, Table S2.). The cellular uptake was below 1% in all cases, indicating that the tested derivatives did not enter the cells in significant amounts (Supplementary material, Table S2.). The recovery of **12** was the lowest (~6%), but it bound the most to BSA (98%) (Supplementary material, Table S2.). The high BSA binding may explain the unusually low recovery since it impedes the LC-MS analysis from the biological samples. **19b** showed the highest recovery (~80%), while its binding to BSA was the lowest (14%). Mass balance above 70% for molecules in drug permeability assays is considered as good. The recovery of **17c** was about ~40% and its binding to BSA was low, similarly to **19b**. The membranes of culture inserts as well as the polystyrene surface of culture plastic ware (12-well plates in our case) may sequester amphiphilic or lipophilic drugs. The same insert type with polyester membrane, as used in our experiment, was shown to adsorb 10% of the triazineaminopiperidine derivative S9788, a modulator of P-glycoprotein activity (Cecchelli et al., 1999). Measured by sorption tests, polystyrene surfaces bound basic drugs in a significant amount resulting in drug loss in the range of 24-65% (Palmgrén et al., 2006). Based on these data we hypothesize that the low recovery of **17c** may be due to sorption to the membrane of the inserts and the polystyrene surfaces of the receiver multiwell plates (Fig. 5.). The recovery values of the tested derivatives through cell-free inserts were also calculated. Only **19b** showed ~100% recovery which means it does not bind to the membrane of the inserts or the plastic surfaces (Supplementary material, Table S3.).

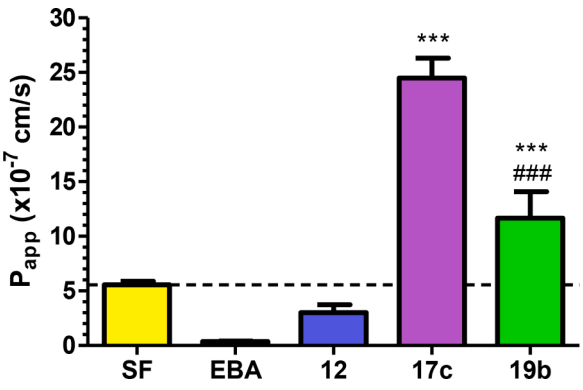

Fig. 7. Permeability of **12, 17c** and **19b** (1 μM) across the culture model of the BBB after 1-hour treatment. P_{app}: apparent permeability coefficient; SF: sodium fluorescein (376 Da); EBA: Evans blue-albumin complex (67 kDa). Mean ± SD, n = 4–6, ANOVA, Bonferroni test, ***p < 0.001 compared to **12**, ###p < 0.001 compared to **17c**.

BSA binding of **12, 17c** and **19b** was verified qualitatively using UV-spectroscopic measurements as we have described DNA binding of other cyclic C_5-curcuminoids (Huber et al., 2019; Huber et al., 2020). Fading maximums and hypsochrom (blue) shifts of **12, 17c** and **19b** were observed depending on different BSA concentrations (Supplementary material, Fig. S3.). Quantification of BSA binding was accomplished by LC-MS (Supplementary material, Table S2.). To our best knowledge, this is the first example describing BSA binding of cyclic C_5-curcuminoids in the corresponding literature.

We observed differences in some of the structure-related, predictable physicochemical parameters of compounds tested as well (Table 3.). Calculated solubility in water is the highest in the case of **19b** which had the highest antiproliferative activity with good BBB permeability. Nevertheless, compound **17c**, which is practically insoluble in water with low protonation at pH = 7.4 shows the best permeability. LogP_{TLC} values and calculated distribution coefficients (CLog*D* at pH = 7.4) are in good agreement with each other. The disagreement between 100% ionized form and relatively good penetration through BBB of **19b** can be explained by the possible involvement of monocarboxylic acid transporters, which are present in cells of the BBB model (Veszelka et al., 2018).

3. Conclusions

We have prepared 21 derivatives (**8-13, 17** and **19-22**) of the cyclic C_5-curcuminoid family for their testing on CNS tumorous cell lines, like human neuroblastoma and astrocytoma cells. Based on cytotoxicity measurements, we revealed that among the 16 highly effective curcuminoids with IC_{50} values in the low nanomolar and picomolar range six compounds, **13, 12, 17b, 17c 17d** and **17e** are good candidates as antitumor agents against astrocytoma, while **19b** and **21** may be suitable for *in vivo* animal studies in case of neuroblastoma. The most promising curcuminoid, based on the viability and IC_{50} values, compound **11** was successful both against neuroblastoma and astrocytoma. Compounds **11** and **19b** have shown the highest cytotoxic selectivity comparing the IC_{50} values received on cancer and non-cancer cells. Cytotoxicity of the tested derivatives did not show strong correlation with their experimental logP_{TLC} values and the optimal logP_{TLC} was in the 1-3 range. Three of the tested cyclic C_5-curcuminoids **12, 17c** and **19b** were subjected to penetration tests through a BBB model. Compounds tested did not damage rat brain endothelial cells in concentrations lower than 10 μM. It turned out, as an interesting novelty, that **17c** and **19b** derivatives can permeate the BBB and their penetration takes place in different ratios. Calculations with the apparent permeability coefficients (P_{app}) suggested that the very small IC_{50} values may allow the relatively fast formation of the effective concentration of compounds **17c** and **19b** behind the BBB. Based on these findings the extra synthetic efforts like the preparation of "PEGylated" (**5**) or polyamine type spermine (**7**) derivatives with special substituents for organ targeting transport can be avoided. We have also described diverse binding abilities of cyclic C_5-curcuminoids **12, 17c** and **19b** to serum albumin.

In this work we have shown that none of the experimental or predictable physicochemical parameters of the compounds tested

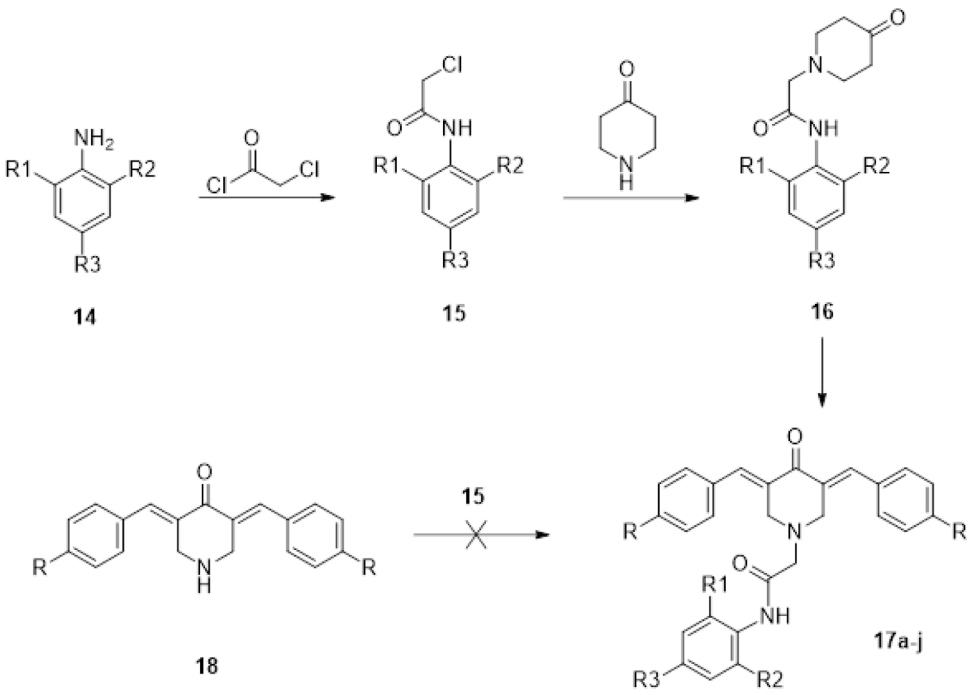

Scheme 1. Synthesis of compounds **17a-j** in a Lidocaine-analogue synthesis followed by a base-catalyzed *Claisen-Schmidt* condensation (**17a**: R = R1 = R2 = R3 = H; **17b**: R = CF_3, R1 = R2 = R3 = H; **17c**: R = Cl, R1 = R2 = R3 = H; **17d**: R = Cl, R1 = R2 = CH_3, R3 = H; **17e**: R = CF_3, R1 = H, R2 = R3 = Cl; **17f**: R = OCH_3, R1 = R2 = R3 = H; **17g**: R = OCH_3, R1 = R2 = CH_3, R3 = H; **17h**: R = OCH_3, R1 = H, R2 = R3 = Cl; **17i**: R = R2 = R3 = Cl, R1 = H; **17j**: R = R1 = H, R2 = R3 = Cl).

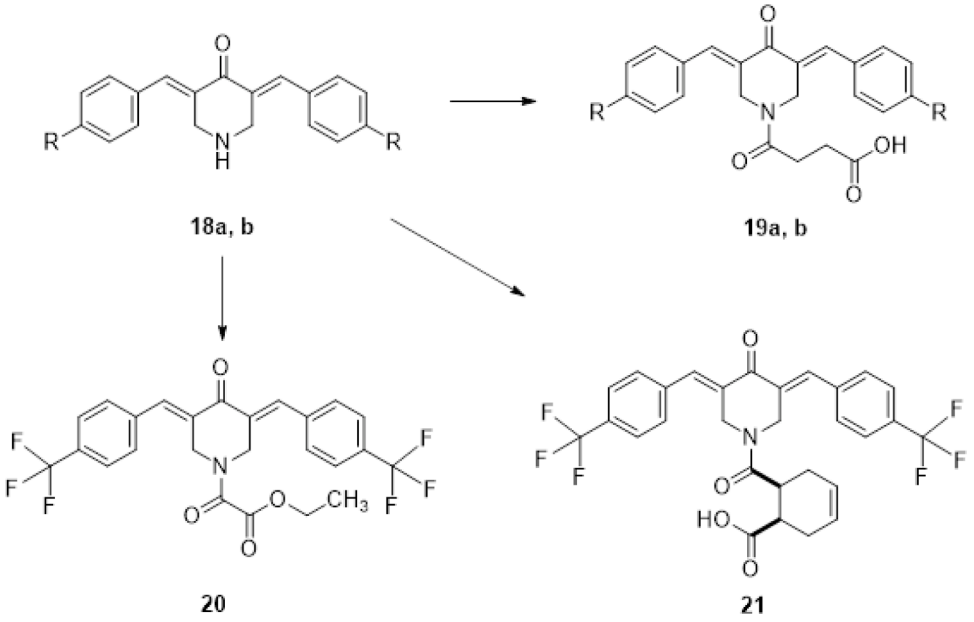

Scheme 2. Synthesis of CLEFMA-analogue compounds **19-21** (**a**: R = Cl; **b**: R = CF_3): **18a** or **18b** was reacted with succinic anhydride for derivatives **19a**, or **19b** respectively, and *cis*-3-cyclohexene-1,2-dicarboxilic acid anhydride for **21**. Ester derivative **20** was prepared from **18b** acylated with ethyl oxalyl chloride in the presence of triethylamine.

correlated to cytotoxicity. This provides indirect evidence on presence of multiple cellular targets of the cross-conjugated ß-dienone system of such compounds. A multivariate approach is necessary to investigate the reversable thia-Michael reaction of such cyclic C_5-curcuminoids with cellular thiols in order to gain more insight to their way of biological action and solubility in water. As a future perspective, we propose here to further investigate the interaction of these curcuminoids with cysteine residues of cellular thiols based on the equilibrium of the reversable thia-Michael reaction.

4. Experimental protocols

4.1. Chemistry

Chemicals, solvents and reagents for the study were purchased from Alfa Aesar, Molar and Merck Ltd (Budapest, Hungary). Melting points were determined on a Barnstead-Electrothermal 9100 apparatus and are uncorrected. Silica gel 60 (0.2-0.5 mm, MERCK) was used for column chromatography and pre-coated silica gel 60 (F-254, MERCK) plates for

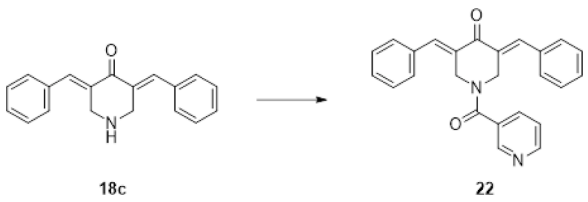

Scheme 3. Synthesis of compound **22**. Compound **18c** was acylated with nicotinoyl chloride in the presence of triethylamine (TEA).

Table 3
Apparent permeability coefficient (P_{app}), IC_{50} data, experimental logP_{TLC} values together with some predictable physicochemical parameters (distribution coefficient, solubility in water, protonation/deprotonation at physiological pH) of compounds **12, 17c** and **19b**. ChemAxon's Marvin Suite (ChemAxon, 2022) was used for calculations.

Compound:	12	17c	19b
P_{app} ($\times 10^{-7}$ cm/sec):	3.01	24.48	11.65
IC_{50} neuroblastoma (nM):	0.99	7.48	0.14
IC_{50} astrocytoma (nM):	0.51	5.65	0.39
Experimental logP_{TLC}:	4.70	5.23	1.41
Clog*D* (pH = 7.4):	6.06	6.87	2.38
Solub./water (mg/L, pH = 7.4):	0.34	0.02	161.73
Protonation (%, pH = 7.4):	0.32	0.02	100*

* acid anion

TLC.

NMR: ^{1}H- and ^{13}C-spectra were recorded with a Bruker Avance III 500 (500.15/125.77 MHz for ^{1}H/^{13}C) spectrometer. Chemical shifts were referenced to the residual solvent signals. Measurements were run at a probe temperature of 298 K in DMSO-d_6 solutions. All the ^{1}H and ^{13}C NMR spectra were in good accordance with the expected structures.

MS: HPLC-MS analyses were performed on a Thermo Dionex Ultimate 3000 liquid chromatograph (Dionex, Sunnyvale, CS, USA) coupled with a Thermo Q Exactive Focus hybrid Quadrupole-Orbitrap mass spectrometer (Thermo Fisher Scientific, Waltham, MA, USA). Data analysis and evaluations were performed using the Q Exactive Focus 2.1 and Xcalibur 4.2. software (Thermo Fisher Scientific). The separation of compounds was performed on a Thermo Hypersil GOLD C_{18} (150 mm × 4.6 mm × 5 μm) analytical column. The mobile phase consisted of 0.1% formic acid solution (A) and methanol with 0.1% formic acid (B). Gradient elution was performed: 0 min 20% B, 6 min 80% B, 8 min 80% B, 10 min 20% B, 10 min stop. Chromatography was performed at 40 °C, the flow rate was 0.3 mL/min. The injected volume was 5 μL. MS measurement was performed in switched ion mode, with the same parameters. The ESI source was operated with a spray voltage of 3.50 kV. The spray voltage was set to 3.5 kV, the capillary temperature to 350 °C. Sheath gas was delivered at 30 AU and temperatured at 450 °C. Aux gas was delivered at 10 AU. Full-range mass spectra (100–1500 m/z) were collected under the optimal conditions.

The physical and analytical data of resynthesized compounds **8-12** are identical to the original ones (Huber et al., 2015, 2019).

4.1.1. (2E,6E)-2,6-Bis[(4'-pyridinyl)methylene]-4-hydroxycyclohexanone (8)

prepared as described in (Huber et al., 2019)

4.1.2. (2E,6E)-2,6-Bis[(3'-pyridinyl)methylene]-4-hydroxycyclohexanone (9)

prepared as described in (Huber et al., 2019)

4.1.3. 1-(α-Chloroacetyl)-(3E,5E)-3,5-bis(4'-methoxybenzylidene)-piperidin-4-one (10)

prepared as described in (Huber et al., 2019)

4.1.4. N-(γ-oxobutyl)-3,5-bis(benzylidene)-4-piperidone (11)

prepared as described in (Huber et al., 2015)

4.1.5. N-(γ-oxobutyl)-3,5-bis(4'-chlorobenzylidene)-4-piperidone (12)

prepared as described in (Huber et al., 2015)

4.1.6. N-(γ-oxobutyl)-3,5-bis(4'-fluorobenzylidene)-4-piperidone (13)

prepared as described in (Huber et al., 2015) from 4-fluorobenzaldehyde. Mp.: 116-117 °C. Yield: 91%.^{1}H-NMR (500 MHz, DMSO-D_6) δ (ppm) 1.99 (s, 3H), 2.53 (m, 2H), 2.74 (m, 2H), 3.73 (s, 4H), 7.32 (m, 4H), 7.49 (m, 4H), 7.69 (s, 2H). ^{13}C-NMR (125 MHz, DMSO-D_6) δ (ppm) 29.6, 40.4, 50.7, 53.6, 115.7 ($^{2}J_{C,F}$ = 21.7 Hz), 122.0, 122.1, 124.6 ($^{2}J_{C,F}$ = 3.4 Hz), 127.03, 127.06, 130.74, 130.75, 131.5 ($^{3}J_{C,F}$ = 8.5 Hz), 135.0, 160.3 ($^{1}J_{C,F}$ = 249 Hz), 186.0, 207.2. MS: m/z for $C_{23}H_{22}F_2NO_2$ $[M+H]^+$ calculated: 382.1613; found: 382.1730

4.1.7. General procedure for the synthesis of compounds 17a-j (base-catalyzed Claisen-Schmidt condensation)

A mixture of 10 mmol of suitable substituted N-(anilinocarbonylmethyl)-piperid-4-one (**16**), 20 mmol of the appropriate arylaldehyde (benzaldehyde, 4-chlorobenzaldehyde, 4-methoxybenzaldehyde or 4-trifluoromethyl-benzaldehyde) and 20 mmol potassium hydroxide in 25 ml dry and gas-free methanol was stirred at room temperature, till the starting materials couldn't be detected on the TLC plate. The reaction mixture was then diluted with 100 ml water. After 10 min of stirring the yellow solid was collected on a glass filter, washed with water three times. The crystalline yellow mass was finally rinsed with methanol. The yellow solid was dried and recrystallized from a suitable solvent, usually from a methanol/chloroform mixture.

4.1.7.1. α-[(2E,6E)-2,6-bisbenzylidene-piperid-4-one-1-yl]-N-phenyl-acetamide (17a). Overall yield: 57%. Mp: 181-182 °C. ^{1}H-NMR (500 MHz, DMSO-D_6) δ (ppm) 3.41 (s, 2H), 4.02 (s, 4H), 7.01 (m, 1H), 7.24 (m, 2H), 7.37-7.53 (br m, 12H), 7.67 (s, 2H). ^{13}C-NMR (125 MHz, DMSO-D_6) δ (ppm) 54.0, 60.2, 119.3, 123.2, 128.4, 128.6, 129.1, 130.2, 133.4, 134.4, 134.9, 138.4, 167.8, 186.2. MS: m/z for $C_{27}H_{25}N_2O_2$ $[M+H]^+$ calculated: 409.1916; found: 409.1909.

4.1.7.2. α-[(2E,6E)-2,6-bis(p-trifluormethyl-benzylidene)-piperid-4-one-1-yl]-N-phenyl-acetamide (17b). Overall yield: 61%. Mp.: 190-191 °C. ^{1}H-NMR (500 MHz, DMSO-D_6) δ (ppm) 3.42 (s, 2H), 4.05 (s, 4H), 7.01 (m, 1H), 7.23 (m, 2H), 7.47 (m, 2H), 7.70 (m, 6H), 7.79 (m, 4H). ^{13}C-NMR (125 MHz, DMSO-D_6) δ (ppm) 53.6, 59.6, 119.3, 123.2, 123.9 (q, $^{1}J_{C,F}$ = 272.3 Hz), 125.28, 125.31, 128.4, 128.8 (q, $^{2}J_{C,F}$ = 31.1 Hz), 130.7, 133.4, 135.4, 138.33, 138.42, 167.7, 186.2. MS: m/z for $C_{29}H_{23}F_6N_2O_2$ $[M+H]^+$ calculated: 545.1664; found: 545.1604

4.1.7.3. α-[(2E,6E)-2,6-bis(p-chlorobenzylidene)-piperid-4-one-1-yl]-N-phenyl-acetamide (17c). Overall yield: 63%. Mp: 203-204 °C. ^{1}H-NMR (500 MHz, DMSO-D_6) δ (ppm) 3.41 (s, 2H), 4.00 (s, 4H), 7.01 (m, 1H), 7.25 (m, 2H), 7.49 (m, 10H), 7.63 (2, 2H). ^{13}C-NMR (125 MHz, DMSO-D_6) δ (ppm) 53.8, 59.9, 119.3, 123.2, 128.4, 128.6, 131.9, 133.2, 133.6, 133.8, 134.0, 138.3, 167.7, 186.1. MS: m/z for $C_{27}H_{23}Cl_2N_2O_2$ $[M+H]^+$ calculated: 477.1137; found: 477.1084.

4.1.7.4. α-[(2E,6E)-2,6-bis(p-chlorobenzylidene)-piperid-4-one-1-yl]-N-(2',6'-dimethylphenyl)-acetamide (17d). Overall yield: 65%. Mp.: 210-211 °C. ^{1}H-NMR (500 MHz, DMSO-D_6) δ (ppm) 1.84 (s, 6H), 3.42 (s, 2H), 3.99 (s, 4H), 6.96 (m, 3H), 7.53 (m, 8H), 7.67 (s, 2H). ^{13}C-NMR (125 MHz, DMSO-D_6) δ (ppm) 17.6, 54.2, 60.1, 126.2, 127.3, 128.6, 131.9, 133.3, 133.6, 133.7, 133.8, 134.6, 135.0, 167.3, 185.7. MS: m/z for $C_{29}H_{27}Cl_2N_2O_2$ $[M+H]^+$ calculated: 505.1450; found: 505.1395.

4.1.7.5. α-[(2E,6E)-2,6-bis(p-trifluormethyl-benzylidene)-piperid-4-one-1-yl]-N-(2',4'-dichlorophenyl)-acetamide (17e). Overall yield: 60%. Mp.:

191-192 °C. ^{1}H-NMR (500 MHz, DMSO-D_6) δ (ppm) 3.48 (s, 2H), 4.08 (s, 4H), 7.34 (dd, J = 2.4 Hz, 8.8 Hz, 1H), 7.57 (d, J = 2.4 Hz, 1H), 7.69-7.77 (br m, 6H), 7.81 (m, 5H). ^{13}C-NMR (125 MHz, DMSO-D_6) δ (ppm) 53.9, 59.6, 123.9 (q, $^1J_{C,F}$ = 272.3 Hz), 124.3, 125.3 (q, $^3J_{C,F}$ = 3.4 Hz), 125.5, 127.5, 128.5, 128.6, 128.9 (q, $^2J_{C,F}$ = 32.1 Hz), 130.8, 133.2, 133.7, 135.1, 138.3, 167.8, 185.9. MS: m/z for $C_{29}H_{21}Cl_2F_6N_2O_2$ $[M+H]^+$ calculated: 613.0884; found: 613.0822.

4.1.7.6. α-[(2E,6E)-2,6-bis(p-methoxybenzylidene)-piperid-4-one-1-yl]-N-phenyl-acetamide (17f). Overall yield: 65%. Mp.: 187-188 °C. ^{1}H-NMR (500 MHz, DMSO-D_6) δ (ppm) 3.15 (s, 2H), 3.80 (s, 6H), 3.99 (s, 4H), 7.01 (m, 5H), 7.25 (m, 2H), 7.46 (m, 4H), 7.50 (m, 2H), 7.61 (s, 2H). ^{13}C-NMR (125 MHz, DMSO-D_6) δ (ppm) 54.2, 55.2, 60.3, 114.2, 119.3, 123.2, 127.1, 128.4, 131.4, 132.2, 134.5, 138.4, 159.9, 167.8, 185.9. MS: m/z for $C_{29}H_{29}N_2O_4$ $[M+H]^+$ calculated: 469.2127; found: 469.2076.

4.1.7.7. α-[(2E,6E)-2,6-bis(p-methoxybenzylidene)-piperid-4-one-1-yl]-N-(2',6'-dimethylphenyl)-acetamide (17g). Overall yield: 66%. Mp.: 194-195 °C. ^{1}H-NMR (500 MHz, DMSO-D_6) δ (ppm) 3.43 (s, 2H), 3.82 (s, 6H), 4.00 (s, 4H), 6.92-7.05 (br m, 7H), 7.47 (m, 4H), 7.64 (s, 2H). ^{13}C-NMR (125 MHz, DMSO-D_6) δ (ppm) 17.6, 54.5, 55.2, 60.4, 114.1, 126.2, 127.1, 127.3, 131.3, 132.2, 134.6, 134.7, 135.0, 160.0, 167.5, 185.6. MS: m/z for $C_{31}H_{33}N_2O_4$ $[M+H]^+$ calculated: 497.2440; found: 497.2385.

4.1.7.8. α-[(2E,6E)-2,6-bis(p-methoxybenzylidene)-piperid-4-one-1-yl]-N-(2',4'-dichlorophenyl)-acetamide (17h). Overall yield: 59%. Mp.: 201-202 °C. ^{1}H-NMR (500 MHz, DMSO-D_6) δ (ppm) 3.50 (s, 2H), 3.80 (s, 6H), 4.02 (s, 4H), 7.01 (d, J = 8.6 Hz, 4H), 7.36 (dd, J = 1.9 Hz, 8.8 Hz, 1H), 7.47 (d, J = 8.6 Hz, 4H), 7.57 (d, J = 1.9 Hz, 1H), 7.63 (s, 2H), 7.91 (d, J = 8.8 Hz, 1H). ^{13}C-NMR (125 MHz, DMSO-D_6) δ (ppm) 54.4, 55.1, 60.1, 114.2, 123.9, 125.1, 127.0, 127.6, 128.4, 128.5, 131.1, 132.3, 133.2, 134.7, 160.0, 168.0, 185.6. MS: m/z for $C_{29}H_{27}Cl_2N_2O_4$ $[M+H]^+$ calculated: 537.1348; found: 537.1295.

4.1.7.9. α-[(2E,6E)-2,6-bis(p-chlorobenzylidene)-piperid-4-one-1-yl]-N-(2',4'-dichlorophenyl)-acetamide (17i). Overall yield: 65%. Mp.: 151-152 °C. ^{1}H-NMR (500 MHz, DMSO-D_6) δ (ppm) 3.49 (s, 2H), 4.03 (s, 4H), 7.36 (dd, J = 2.3 Hz, 8.8 Hz, 1H), 7.46-7.56 (br m, 8H), 7.58 (d, J = 2.3 Hz, 1H), 7.65 (s, 2H), 7.85 (d, J = 8.8 Hz, 1H). ^{13}C-NMR (125 MHz, DMSO-D_6) δ (ppm) 54.1, 59.8, 124.3, 125.4, 127.6, 128.5, 128.6, 132.0, 133.17, 133.24, 133.7, 133.87, 133.91, 133.92, 167.9, 185.8. MS: m/z for $C_{27}H_{21}Cl_4N_2O_2$ $[M+H]^+$ calculated: 545.0357; found: 545.0303.

4.1.7.10. α-[(2E,6E)-2,6-bisbenzylidene-piperid-4-one-1-yl]-N-(2',4'-dichlorophenyl-acetamide (17j). Overall yield: 65%. Mp.: 120-121 °C. ^{1}H-NMR (500 MHz, DMSO-D_6) δ (ppm) 3.50 (s, 2H), 4.06 (s, 4H), 7.35 (dd, J = 2.4 Hz, 8.8 Hz, 1H), 7.37-7.52 (br m, 10H), 7.56 (d, J = 2.4 Hz, 1H), 7.69 (s, 2H), 7.85 (d, J = 8.8 Hz, 1H). ^{13}C-NMR (125 MHz, DMSO-D_6) δ (ppm) 54.3, 59.9, 124.2, 125.4, 127.5, 128.5, 128.6, 129.1, 130.3, 133.16, 133.23, 134.3, 135.1, 167.9, 185.9. MS: m/z for $C_{27}H_{23}Cl_2N_2O_2$ $[M+H]^+$ calculated: 477.1137; found: 477.1087.

4.1.8. General procedure for the synthesis of compounds 19a,b and 21 (acylation with acid anhydrides)

Compound **18a** or **18b** (5 mmol) was dissolved in a mixture of 15 ml dry dichloromethane and triethylamine (10 mmol). The corresponding acid anhydride (5 mmol) was added in one portion under stirring at room temperature. Stirring was continued till the starting materials couldn't be detected on the TLC plate. After completion of the reaction, the mixture was diluted with 20 ml of water, extracted 3 × 15 ml of dichloromethane at pH~4/HCl. The combined organic layers dried (Na_2SO_4 sicc) and evaporated, the crude yellow product was recrystallized from a suitable solvent, usually methanol.

4.1.8.1. 4-[(3'E,5'E)-3',5'-bis(p-chlorobenzylidene)-piperid-4'-one-1'-yl]-4-oxobutane-1-carboxylic acid (19a). Prepared from compound **18a** and succinic anhydride. Yield: 71%. Mp.: 196-197 °C. ^{1}H-NMR (500 MHz, DMSO-D_6) δ (ppm) 2.31 (m, 2H), 2.41 (m, 2H), 4.82 (m, 4H), 7.52-7.63 (br m, 8H), 7.69 (s, 2H). ^{13}C-NMR (125 MHz, DMSO-D_6) δ (ppm) 26.9, 28.5, 42.3, 45.8, 128.7, 128.8, 132.08, 132.24, 132.79, 132.86, 133.05, 134.16, 134.24, 134.8, 169.9, 173.5, 185.8. MS: m/z for $C_{23}H_{20}Cl_2NO_4$ $[M+H]^+$ calculated: 444.0769; found: 444.0742.

4.1.8.2. 4-[(3'E,5'E)-3',5'-bis(p-trifluormethyl-benzylidene)-piperid-4'-one-1'-yl]-4-oxobutane-1-carboxylic acid (19b). Prepared from compound **18b** and succinic anhydride. Yield: 65%. Mp.: 164-165 °C. ^{1}H-NMR (500 MHz, DMSO-D_6) δ (ppm) 2.31 (m, 2H), 2.42 (m, 2H), 4.85 (m, 4H), 7.71-7.88 (br m, 10H). ^{13}C-NMR (125 MHz, DMSO-D_6) δ (ppm) 26.8, 28.5, 42.2, 45.7, 123.9 (q, $^1J_{C,F}$ = 272 Hz), 125.4, 129.1 (q, $^2J_{C,F}$ = 32.6 Hz), 130.8, 130.9, 134.2, 134.4, 134.5, 138.0, 138.2, 170.0, 173.4, 185.9. MS: m/z for $C_{25}H_{20}F_6NO_4$ $[M+H]^+$ calculated: 512.1297; found: 512.1263.

4.1.8.3. cis-6-[(3'E,5'E)-3',5'-bis(p-trifluormethyl-benzylidene)-piperid-4'-one-1'-carbonyl]-3-cyclohexene-1-carboxylic acid (21). Prepared from compound **18c** and cis-3-cyclohexene-1,2-dicarboxilic acid anhydride. Yield: 69%. Mp.: 178-179 °C. ^{1}H-NMR (500 MHz, DMSO-D_6) δ (ppm) 1.89 (m 1H), 1.96 (m, 2H), 2.39 (m, 1H), 2.48 (m, 1H), 3.12 (m, 1H), 4.85 (m, 4H), 5.41 (d, J = 10.1 Hz, 1H), 5.50 (d, J = 10.1 Hz, 1H), 7.88 (m, 6H), 7.85 (m, 4H). ^{13}C-NMR (125 MHz, DMSO-D_6) δ (ppm) 25.1, 25.5, 34.6, 38.4, 42.5, 46.1, 123.2, 123.9 (q, $^1J_{C,F}$ = 272.2 Hz), 125.45, 125.47, 125.51, 129.1 (q, $^2J_{C,F}$ = 31.6 Hz), 130.9, 134.47, 134.54, 138.1, 171.9, 174.2, 185.6. MS: m/z for $C_{29}H_{24}F_6NO_4$ $[M+H]^+$ calculated: 564.1610; found: 564.1572.

4.1.9. General procedure for the synthesis of compounds 20 and 22 (acylation with acid chlorides): Compound 18b or 18c (1 mmol) was dissolved in a mixture of 25 ml dry toluene and triethylamine (4 mmol) with gentle heating

The corresponding acid chloride (1 mmol) was added in one portion under stirring with the simultaneous removal of heating. Stirring was continued till the starting materials couldn't be detected on the TLC plate. After completion of the reaction, the mixture was diluted with 20 ml of water, extracted 3 × 15 ml of chloroform. The combined organic layers dried (Na_2SO_4 sicc) and evaporated, the crude yellow product was recrystallized from a suitable solvent, usually methanol.

4.1.9.1. Ethyl 2-[(3'E,5'E)-3',5'-bis(p-trifluormethyl-benzylidene)-piperid-4'-one-1'-yl]-2-oxoethane-1-carboxylate (20). Prepared from compound **18b** and ethyl oxalyl chloride. Yield: 66%. Mp.: 176-177 °C. ^{1}H-NMR (500 MHz, DMSO-D_6) δ (ppm) 0.82 (s, 3H), 3.87 (m, 2H), 4.75 (s, 2H), 4.91 (s, 2H), 7.72 (m, 2H), 7.80 (m, 2H), 7.82-7.91 (m, 6H). ^{13}C-NMR (125 MHz, DMSO-D_6) δ (ppm) 13.0, 41.8, 45.7, 61.9, 123.9 (q, $^1J_{C,F}$ = 272.3 Hz), 125.5, 129.4 (q, $^2J_{C,F}$ = 32.4 Hz), 130.8, 131.0, 132.9, 133.1, 135.3, 136.0, 137.8, 137.9, 159.6, 161.7, 184.8. MS: m/z for $C_{25}H_{20}F_6NO_4$ $[M+H]^+$ calculated: 512.1297; found: 512.1260.

4.1.9.2. (3E,5E)-3,5-bis(p-trifluormethyl-benzylidene)-1-nicotinoyl-piperid-4-one (22). Prepared from compound **18c** and nicotinoyl chloride. Yield: 71%. Mp: 182-183 °C. ^{1}H-NMR (500 MHz, DMSO-D_6) δ (ppm) 4.70 (s, 2H), 5.03 (s, 2H), 7.09 (dd, J = 4.9 Hz, 7.4 Hz, 1H), 7.22-7.86 (br m, 14H), 8.44 (dd, J = 1.5 Hz, 4.9 Hz, 1H), 8.46 (d, J = 1.5 Hz, 1H). ^{13}C-NMR (125 MHz, DMSO-D_6) δ (ppm) 43.2, 47.6, 122.8, 128.6, 129.5, 129.9, 130.3, 130.4, 132.0, 134.0, 136.1, 136.9, 147.2, 150.4, 166.9, 185.4. MS: m/z for $C_{25}H_{21}N_2O_2$ $[M+H]^+$ calculated: 381.1603; found: 381.1600.

4.2. Materials and methods for cytotoxicity assays

4.2.1. Cell cultures

The SH-SY5Y, human neuroblastoma cell line (ATCC CRL-2266) was maintained in Dulbecco's Modified Eagle Medium:Nutrient Mixture F-12 Ham (DMEM:F12) culture medium (Lonza Ltd., Basel, Switzerland). The medium was supplemented with 10% fetal bovine serum (FBS, EuroClone, S.p.A, Pero, Italy), 1% non-essential amino acid solution (NEAA, Lonza Ltd.), 1% penicillin/streptomycin (P/S, Lonza Ltd.). The CCF-STTG1, human grade IV astrocytoma cell line (ATCC CRL-1718) was cultured in Roswell Park Memorial Institute (RPMI)-1640 medium (Lonza Ltd.) supplemented with 10% FBS and 0.5% P/S. The C8-D1A, mouse astrocyte cell line (ATCC CRL-2541) and the Cos-1, green monkey kidney fibroblast-like cell line (ATCC CRL-1650) were cultured in DMEM (Lonza Ltd.) supplemented with 10% FBS and 1% P/S.

4.2.2. Cell viability assay

The SH-SY5Y, CCF-STTG1, C8D1A and Cos-1 cells were seeded onto 96-well plates using 5×10^3 cells/well in quintuplicates according to the different curcuminoids and treatment concentrations. The cells were maintained in an antibiotic-free culture medium for 24 h. Each cell line was treated the same way with the synthetized cyclic C_5-curcuminoids (**8-13, 17a-j, 19a,b** and **20-22**) solved in 100% dimethyl sulfoxide (DMSO, Sigma-Aldrich Kft., Budapest, Hungary). Each of the curcuminoids was used in increasing concentrations (1 μM–10 μM; 10 nM - 1 μM and 0.1 nM - 10 nM) for 48 h. DMSO treatment was used as controls in the same way as the curcuminoids. Cisplatin was used as positive control of the experiments. The viability of the aforementioned cell lines was determined using Cell Counting Kit-8 (CCK-8) cell viability assay kit (Sigma-Aldrich Kft., Budapest, Hungary). DMSO treated cells were used as controls of the curcuminoid treated cells. The highest DMSO concentration did not exceed 0.1% in treatment. After the treatments 10 μL of WST-8 reagent was added to each well, then the plates were incubated for 1 h at 37 °C and 5 % CO_2. To stop the reaction, 10 μL of 1% sodium dodecyl sulfate (SDS, Molar Chemicals Kft., Halásztelek, Hungary) was added to each well. The optical density of the samples was measured at 450 nm using a MultiSkan GO microplate spectrophotometer (Thermo Fisher Scientific Inc., Waltham, MA). Viabilities of the different cell lines and treatments were expressed as the percentile of the total cell number of the appropriate DMSO controls. The half-maximal inhibitory concentration (IC_{50}) values were calculated from the cell viability results using GraphPad Prism 8 software (GraphPad Software, San Diego, CA).

4.3. LogP determination and calculation of predictable physicochemical parameters

RP-TLC logP determinations were performed by a slight modification of the previously optimized RP-TLC method used for the determination of some chalcones and cyclic chalcone analogs (Huber et al., 2020). Compounds of the calibration set, selected chalcones and cyclic chalcone derivatives, were synthesized and purified as described (see the structures in "Supportive material" of (Huber et al., 2020)). Two compounds of the validation set (progesterone, diazepam) were of pharmacopoeial grade. All other reagents used were of analytical grade.

RP-TLC determination of the logP of the cyclic C_5-curcuminoid compounds was performed on 20 cm x 20 cm plates precoated with 0.25 mm layers of silanized silica gel $60F_{254}$ (Merck, Germany; #5747). Before using the plates were washed with methanol and dried. The samples were dissolved in 1:1 methanol-chloroform (1 mg/ml) and 2 μl of these solutions was spotted on the plate. Methanol-water, 70 + 30 (v/v), was used as mobile phase. The paper-lined chromatographic chamber was saturated with mobile phase for 30 min before use. After development (150 mm) the plates were dried and the chromatograms were assessed visually under UV illumination ($\lambda = 254$ nm). Three TLC determinations were performed for each substance.

The optimized chromatographic system underwent validation prior to logP measurements. For this purpose, four molecules (progesterone, diazepam, chalcone and a chalcone derivative (Q-693) with known logP values were tested. Comparison of their $logP_{TLC}$ values obtained in this work with previously published experimental logP data resulted in rather good agreement. Thus, these four compounds were also added to the calibration set.

The calculation of predictable physicochemical parameters was performed using ChemAxon's software (ChemAxon, 2022). The log*D* represents the octanol-water coefficient of compounds at a given p*H* value. In details the distribution coefficient is the ratio of the sum of the concentrations of all species of the given compound in octanol to the sum of the concentrations of all species of the compound in water. We have used the general options with the electrolyte (Na+, K+, Cl-) concentrations. ChemAxon's log*P* calculations are based on the fragmentation method. The log*P* value of the given molecule is the sum of the unique fragment's values, respectively. Dipole moment describes the charge separation in a molecule. ChemAxon's plugin calculates the total dipole moment of a given molecule as a vector that depends on the molecular geometry and the atomic partial charges.

4.4. Materials and methods for BBB penetration of compounds 12, 17c and 19b

All reagents were purchased from Sigma-Aldrich Kft., Hungary, unless otherwise indicated.

4.4.1. Working solutions - 12, 17c and 19b

Stock solutions of 10 mM were prepared in DMSO (Supplementary material, Fig. S4.). Working solutions were diluted in culture medium in the 0.1-100 nM and 0.1-30 μM concentration ranges for cell viability experiments. The culture medium contained 10% plasma-derived bovine serum (First Link, Wolverhampton, UK), 10 mM HEPES, 5 μg/ml insulin, 5 μg/ml transferrin, 5 ng/ml sodium selenite (Pan Biotech, Germany), 100 μg/ml heparin, 1 ng/ml basic fibroblast growth factor (Roche, Basel, Switzerland) and 50 μg/ml gentamycin in DMEM/HAM's F-12 (Gibco, Life Technologies, Carlsbad, CA, USA). For the permeability experiment, working solutions were diluted in Ringer-Hepes containing 1% BSA at 1 μM concentration based on the cell viability data.

4.4.2. Cell viability measurements by real-time cell microelectronic sensing

Primary cultures of rat brain endothelial cells for cell viability measurements were prepared as described in our previously published papers (Veszelka et al., 2018; Nakagawa et al., 2009; Veszelka et al., 2013). To measure cell response, we used an RTCA-SP instrument (Agilent, Santa Clara, CA, USA). This impedance-based label-free technique has been used by our team for dynamic monitoring of living cells and non-invasive quantification of adherent cell proliferation and viability (Kiss et al., 2014). The RTCA-SP system utilizes 96-well plates containing gold microelectronic sensor arrays (Agilent, Santa Clara, CA, USA). The interaction between cells and electrodes generates an impedance response that correlates linearly with cell number, adherence and cell growth. This method is more sensitive and informative than colorimetric end-point assays to test damage or functional changes in brain endothelial cells (Harazin et al., 2018). The E-plates were coated with collagen IV and fibronectin solution for 20 min at 37 °C. Culture medium (50 μL) was added to each well for background readings then 50 μl rat brain endothelial cell suspension was dispensed at the density of 6×10^3 cells/well. The cells in the E-plate were kept in an incubator at 37 °C and monitored every 5 min. The cell index at each time point was defined as (Rn–Rb)/15, where Rn is the cell–electrode impedance of the well when it contains cells and Rb is the background impedance of the well with the medium alone. The cells were grown for 3-5 days until reaching confluency which is registered as a plateau phase of the cell index, then were treated with the compounds for 48 h.

4.4.3. Primary cell cultures and blood-brain barrier model for permeability studies

Isolation of rat primary brain endothelial cells, glia and pericytes, and the construction of the in vitro BBB model were performed according to the method described in our previous studies (Veszelka et al., 2018; Nakagawa et al., 2009). After isolation cells were seeded on culture dishes (Corning, Costar, New York, NY, USA) coated with 100 μg/ml collagen type IV and 100 μg/ml fibronectin in sterile distilled water. Brain endothelial cells were cultured in DMEM/HAM's F-12 (Gibco, Life Technologies, Carlsbad, CA, USA), 15% plasma-derived bovine serum (PDS, First Link, Wolverhampton, UK), 100 μg/ml heparin, medium supplement with 5 μg/ml insulin, 5 μg/ml transferrin, 5 ng/ml sodium selenite (ITS, Pan-Biotech Gmbh., Germany), 1 ng/ml basic fibroblast growth factor (bFGF, Roche, Basel, Switzerland) and 50 μg/ml gentamycin. During the first three days of culture, the medium of brain endothelial cells contained 3 μg/ml puromycin to eliminate P-glycoprotein negative, contaminating cell types (Perrière et al., 2005). Primary rat brain pericytes were isolated using the same method as for brain endothelial cells, except that pericytes were plated onto uncoated culture dishes and did not receive puromycin. Primary cultures of rat glial cells were prepared from one-day-old Wistar rats and passaged to 12-well plates (Corning, Costar, New York, NY, USA) coated with collagen type IV (100 μg/ml in sterile distilled water). Rat glial cells were cultured for two weeks before using them for the co-culture model. Pericytes and glial cells were cultured in DMEM/HAM's F-12 supplemented with 10% FBS (Pan-Biotech GmbH) and 50 μg/ml gentamycin. To prepare the co-culture model, pericytes at P2 were passaged to the collagen IV coated bottom side of tissue culture inserts (Transwell, PET membrane, 0.4 μm pore size, Corning Costar) and brain endothelial cells were seeded to the upper side of the collagen IV and fibronectin-coated upper culture insert membranes. Then the inserts containing brain endothelial cells and pericytes on the two sides of the membrane were placed to 12-well plates in which glial cells were grown at the bottom. Both the upper and lower fluid compartments of this system received endothelial culture medium supplemented with 550 nM hydrocortisone and the three types of cells were cultured together for four days before permeability experiments (Veszelka et al., 2018; Nakagawa et al., 2009).

4.4.4. Measurement of the integrity of the paracellular barrier

TEER shows the permeability of intercellular tight junctions therefore it is a key parameter to validate barrier tightness in cell culture models. TEER reflecting the flux of mainly sodium ions through cell layers in culture conditions was measured by Epithelial-volt-ohm meter and STX-2 electrodes (World Precision Instruments, USA), and expressed relative to the surface area of the monolayers ($\Omega \times cm^2$). The values of cell-free inserts were subtracted. TEER was measured every day until the experiment.

4.4.5. Permeability experiment

For the measurement of the permeability of **12, 17c** and **19b** in the apical to basal direction, the culture inserts were transferred to 12-well plates containing 1500 μl 1% BSA-Ringer-Hepes buffer (150 mM NaCl, 2.2 mM $CaCl_2$, 0.2 mM $MgCl_2$, 5.2 mM KCl, 2.8 mM glucose, 6 mM $NaHCO_3$ and 5 mM Hepes, pH 7.4) in the basal (acceptor) compartments. In the apical (donor) compartments culture medium was replaced by 500 μl buffer containing the different curcuminoid derivatives in 1 μM concentrations. To test the function of our BBB model, the flux of permeability marker molecules (sodium fluorescein, 376 Da and Evans blue labelled serum albumin, 67 kDa) was determined across the endothelial monolayers. The plates were kept at 37 °C in an incubator with 5% CO_2 for 1 h on a rocking platform (~100 rpm). After incubation samples from the bottom and upper compartments were collected in low retention tubes. After the transfer assay, rat brain endothelial cells on the insert membranes were dissolved in 250 μl distilled water, then 750 μl abs. ethanol was added. The concentration of the tested compounds was measured by LC-MS (see point *4.5.*).

4.4.6. Calculation of apparent permeability coefficients

The apparent permeability coefficients (P_{app}) were calculated as described in our previous paper (Bocsik et al., 2016). Cleared volume was calculated from the concentration difference of the derivatives in the basal (acceptor) compartment ($[C]_B$) after 1 h and apical (donor) compartments at 0 hours ($[C]_A$), the volume of the basal (acceptor) compartment (V_B; 1.5 ml) and the surface area available for permeability (A; 1.12 cm^2) by the following equation (Váradi et al., 2017):

$$P_{app} = \frac{[C]_B \times V_B}{A \times [C]_A \times t}$$

4.4.7. Calculation of mass balance

The mass balance was calculated from the concentration of the **12, 17c** and **19b** in the apical (donor) compartment (C_{fA}), the basal (acceptor) compartment (C_{fB}) and the initial concentration of the treating solutions in the apical (donor) compartment (C_{0A}), the volume of the apical (donor) (V_A; 0.5 ml) and basal (acceptor) compartment (V_B; 1.5 ml) by the following equation (Hellinger et al., 2012):

$$\%\text{Mass balance} = \frac{C_{fA}V_A + C_{fB}V_B}{C_{0A}V_A} \text{x} 100\%$$

The mass balance was corrected with the concentrations of **12, 17c** and **19b** in the cells.

4.4.8. Statistical analysis

All data presented are means ± SD. The values were compared using one-way ANOVA followed by the Bonferroni test using GraphPad Prism 5.0 software (GraphPad Software Inc., USA). Changes were considered statistically significant at $P < 0.05$.

4.5. Bovine serum albumin (BSA) binding measurements

4.5.1. Qualitative UV spectroscopic

UV-vis measurements were performed on Jasco V-670 (Japan) spectrophotometer using 1 cm path length quartz cuvettes at ambient temperature.

For BSA binding studies, stock solution of BSA (Sigma-Aldrich Hungary, Budapest) (50 μM) was prepared by dissolving BSA in sodium phosphate buffer (0.1 M, pH 7.4). Variation in the absorption spectrum of BSA (10 μM) has been studied as a function of chalcone concentration from 0 to 20 μM. Investigated compounds were dissolved in DMSO immediately before usage. The freshly prepared solutions were diluted with 0.1 M sodium phosphate solution (pH 7.4) to the final concentrations (0 – 20 μM). The concentration of DMSO in the mixtures was 1% v/v. Measurements were performed in the presence of BSA (10 μM) after 30 min equilibration at 37 °C in the dark.

4.5.2. Quantitative LC-MS

The integrated high-performance liquid chromatography system (Thermo Dionex UltiMate 3000 HPLC) was coupled with an Orbitrap high-resolution accurate-mass mass spectrometer system (Thermo Q Exactive Focus quadrupole-Orbitrap hybrid MS).

Separation of compounds was performed on a 3 mm x 75 mm, 1.6 μm particle size, Cortecs UPLC Phenyl analytical column. The eluent 'A' was 0,1% formic acid in water and the eluent 'B' was 0,1% formic acid in acetonitrile. A gradient elution was performed: 0 min 30% B, 6 min 80% B, 8 min 80% B, 10 min 30% B, 10 min stop. Chromatography was performed at 40 °C, the flow rate was 0.3 mL/min. The injected volume was 5 μL. The mass spectrometer was equipped with a heated electrospray ion source which was operated in the positive ion mode. The spray voltage was set to 4.5 kV, the capillary temperature set to 200 °C. Sheath gas was delivered at 25 L/hour and temperatured at 400 °C. Aux gas was delivered at 5 L/hour. Mass range was set to m/z 300–600. Data analysis was performed using the Thermo Xcalibur (version 4.1) software.

Declaration of Competing Interest

The authors declare that they have no known competing financial interests or personal relationships that could have appeared to influence the work reported in this paper.

Supplementary materials

Supplementary material associated with this article can be found, in the online version, at doi:10.1016/j.ejps.2022.106184.

References

Koehn, F.E., Carter, G.T., 2005. The evolving role of natural products in drug discovery. Nat. Rev. Drug Discov. 4, 206–220.

Gupta, S.C., Patchva, S., Aggarwal, B.B., 2013. Therapeutic roles of curcumin: lessons learned from clinical trials. AAPS J. 15 (1), 195–218.

Oliveira, A.S., Sousa, E., Vasconcelos, M.H., Pinto, M., 2015. Curcumin: a natural lead for potential new drug candidates. Curr. Med. Chem. 22, 4196–4232.

Aggarwal, B.B., Kumar, A., Bharti, A.C., 2003. Anticancer potential of curcumin: preclinical and clinical studies. Anticancer Res. 23, 363–398.

Masuda, T., Jitoe, A., Isobe, J., Nakatani, N., Yonemori, S., 1993. Anti-oxidative and anti-inflammatory curcumin-related phenolics from rhizomes of Curcuma domestica. Phytochemistry 32, 1557–1560.

Kohyama, A., Yamakoshi, H., Hongo, S., Kanoh, N., Shibata, H., Iwabuchi, Y., 2015. Structure-activity relationships of the antitumor C_5-curcuminoid GO-Y030. Molecules 20, 15374–15391.

Liang, G., Shao, L., Wang, Y., Zhao, C., Chu, Y., Xiao, J., Zhao, Y., Li, X., Yang, S., 2009. Exploration and synthesis of curcumin analogues with improved structural stability both in vitro and in vivo as cytotoxic agents. Bioorg. Med. Chem. 17, 2623–2631.

Dahmke, I.N., Boettcher, S.P., Groh, M., Mahlknecht, U., 2014. Cooking enhances curcumin anti-cancerogenic activity through pyrolytic formation of "deketene curcumin. Food Chem. 151, 514–519.

Yoshida, T., Maruyama, T., Miura, M., Inoue, M., Fukuda, K., Shimazu, K., Taguchi, D., Kanda, H., Oshima, M., Iwabuchi, Y., Shibata, H., 2018. Dietary intake of pyrolyzed deketene curcumin inhibits gastric carcinogenesis. J. Funct. Foods 50, 192–200.

Calculator Plugins were used in this research for structure-property prediction and physicochemical calculations, Marvin Suite version 15.2, 23, 2022. ChemAxon. http://www.chemaxon.com.

Das, U., Sharma, R.K., Dimmock, J.R., 2009. 1,5-Diaryl-3-oxo-1,4-pentadienes: A case for antineoplastics with multiple targets. Curr. Med. Chem. 16, 2001–2020.

Editor Huber, I., Perjési, Pál, 2020. Synthesis, some physicochemical characteristics and biological activities of C_5-curcuminoids (review). Chalcones and their synthetic analogs. Nova Science Publishers Inc, pp. 285–333. EditorISBN: 978-1-53618-709-0pp.

Lotfy, G., Said, M.M., El Ashry, S.H., El Tamany, S.H., Abdel Aziz, Y.M., Soliman, S.M., Al-Majid, A.M., Ghabbour, H.A., Barakat, A., 2019. Syntheses and X-ray crystal structures combined with conformational and Hirshfeld analyses of chalcones based on a cyclohexanone scaffold. J. Mol. Struct. 1198, 1268732.

Jiang, J.L., Jin, X.L., Zhang, H., Su, X., Qiao, B., Yuan, Y.J., 2012. Identification of antitumor constituents in curcuminoids from *Curcuma longa* L. based on the composition-activity relationship. J. Pharm. Biomed. Anal. 70, 664–670.

Kohyama, A., Fukuda, M., Sugiyama, S., Yamakoshi, H., Kanoh, N., Ishioka, C., Shibatac, H., Iwabuchi, Y., 2016. Reversibility of the *thia*-Michael reaction of cytotoxic C_5-curcuminoid and structure–activity relationship of bis-thiol-adducts thereof. Org. Biomol. Chem. 14, 10683–10687.

Mapoung, S., Suzuki, S., Fuji, S., Naiki-Ito, A., Kato, H., Yodkeeree, S., Ovatlarnporn, C., Takahashi, S., Limtrakul, P., 2019. Cyclohexanone curcumin analogs inhibit the progression of castration-resistant prostate cancer *in vitro* and *in vivo*. Cancer Sci. 110, 596–607.

Das, S., Das, U., Michel, D., Gorecki, D.K.J., Dimmock, J.R., 2013. Novel 3,5-bis(arylidene)-4-piperidone dimers: potent cytotoxins against colon cancer cells. Eur. J. Med. Chem. 64, 321–328.

Santiago-Vazquez, Y., Das, S., Das, U., Robles-Escajeda, E., Ortega, N.M., Lema, C., Varela-Ramírez, A., Aguilera, R.J., Balzarini, J., De Clercq, E., Dimmock, S.G., Gorecki, D.K.J., Dimmock, J.R., 2014. Novel 3,5-bis(arylidene)-4-oxo-1-piperidinyl dimers: Structure activity relationships and potent antileukemic and antilymphoma cytotoxicity. Eur. J. Med. Chem. 77, 315–322.

Zhang, Y., Liu, Z., Wu, J., Bai, B., Chen, H., Xiao, Z., Chen, L., Zhao, Y., Lum, H., Wang, Y., Zhang, H., Liang, G., 2018. New MD2 inhibitors derived from curcumin with improved anti-inflammatory activity. Eur. J. Med. Chem. 148, 291–305.

Liu, G.Y., Jia, C.C., Han, P.R., Yang, J., 2018. 3,5-Bis(2-fluorobenzylidene)-4-piperidone induce reactive oxygen species-mediated apoptosis in A549 cells. Med. Chem. Res. 27, 128–136.

Yuan, X., Li, H., Bai, H., Su, Z., Xiang, Q., Wang, C., Zhao, B., Zhang, Y., Zhang, Q., Chu, Y., Huang, Y., 2014. Synthesis of novel curcumin analogues for inhibition of 11b-hydroxysteroid dehydrogenase type 1 with anti-diabetic properties. Eur. J. Med. Chem. 77, 223–230.

Anchoori, R.K., Karanam, B., Peng, S., Wang, J.W., Jiang, R., Tanno, T., Orlowski, R.Z., Matsui, W., Zhao, M., Rudek, M.A., Hung, C., Chen, X., Walters, K.J., Roden, R.B.S., 2013. A bis-Benzylidine piperidone targeting proteasome ubiquitin receptor RPN13/ADRM1 as a Therapy for Cancer. Cancer Cell 24, 791–805.

Yang, J.S., Lin, R.C., Hsieh, Y.H., Wu, H.H., Li, G.C., Lin, Y.C., Yang, S.F., Lu, K.H., 2019. CLEFMA activates the extrinsic and intrinsic apoptotic processes through JNK1/2 and p38 pathways in human osteosarcoma cells. Molecules 24 (18), 3280–3291.

Sahoo, K., Dozmorov, M.G., Anant, S., Awasthi, V., 2012. The curcuminoid clefma selectively induces cell death in H441 lung adenocarcinoma cells via oxidative stress. Investig. New Drugs 30, 558–567.

Innao, V., Rizzo, V., Allegra, A.G., Musolino, C., Allegra, A., 2021. Promising anti-mitochondrial agents for overcoming acquired drug resistance in multiple myeloma. Cells 10, 439–457.

Bazzaro, M., Linder, S., 2020. Dienone compounds: targets and pharmacological responses. J. Med. Chem. 63 (24), 15075–15093.

Aravindan, S., Natarajan, M., Awasthi, V., Herman, T.S., Aravindan, N., 2013. Novel synthetic monoketone transmute radiation-triggered NFκB dependent TNFα cross-signaling feedback maintained NFκB and favors neuroblastoma regression. PLoS ONE 8, e72464. https://doi.org/10.1371/journal.pone. 00724687.

Simoni, E., Bergamini, C., Fato, R., Tarozzi, A., Bains, S., Motterlini, R., Cavalli, A., Bolognesi, M.L., Minarini, A., Hrelia, P., Lenaz, G., Rosini, M., Melchiorre, C., 2010. Polyamine conjugation of curcumin analogues toward the discovery of mitochondria-directed neuroprotective agents. J. Med. Chem. 53, 7264–7268.

Mufti, S., Bautista, A., Pino-Figueroa, A., 2015. Evaluation of the Neuroprotective Effects of Curcuminoids on B35 and SH-SY5Y Neuroblastoma Cells. Med. Aromat. Plants 4 (3), 197–204. https://doi.org/10.4172/2167-0412.1000197.

Cersosimo, U., Sgorbissa, A., Foti, C., Drioli, S., Angelica, R., Tomasella, A., Picco, R., Semrau, M.S., Storici, P., Benedetti, F., Berti, F., Brancolini, C., 2015. Synthesis, characterization, and optimization for in vivo delivery of a nonselective isopeptidase inhibitor as new antineoplastic agent. J. Med. Chem. 58, 1691–1704.

Shabaninejad, Z., Pourhanifeh, M.H., Movahedpour, A., Mottaghi, R., Nickdasti, A., Mortezapour, E., Shafiee, A., Hajighadimi, S., Moradizarmehri, S., Sadeghian, M., Mousavi, S.M., Mirzaei, H., 2020. Therapeutic potentials of curcumin in the treatment of glioblastoma. Eur. J. Med. Chem. 188, 112040.

Huber, I., Zupkó, I., Kovács, I.J., Minorics, R., Gulyás-Fekete, G., Maász, G., Perjési, P., 2015. Synthesis and antiproliferative activity of cyclic arylidene ketones: a direct comparison of monobenzylidene and dibenzylidene derivatives. Monatsch. Chem. 146, 973–981.

Huber, I., Zupkó, I., Gyovai, A., Horváth, P., Kiss, E., Gulyás-Fekete, G., Schmidt, J., Perjési, P., 2019. A novel cluster of C_5-curcuminoids: design, synthesis, in vitro antiproliferative activity and DNA binding of bis(arylidene)-4-cyclanone derivatives based on 4-hydroxycyclohexanone scaffold. Res. Chem. Intermed. 45, 4711–4735.

Huber, I., Rozmer, Zs., Gyöngyi, Z., Budán, F., Horváth, P., Kiss, E., Perjési, P., 2020. Structure activity relationship analysis of antiproliferative cyclic C_5-curcuminoids without DNA binding: design, synthesis, lipophilicity and biological activity. J. Mol. Struct. 1206, 127661.

Watson, D.G., 2011. Local anaesthetics. Pharmaceutical Chemistry. Elsevier Ltd, pp. 297–305. D.G. WatsonISBN 978-0-443-07233-8pp.

Veszelka, S., Tóth, A., Walter, F.R., Tóth, A.E., Gróf, I., Mészáros, M., Bocsik, A., Hellinger, É., Vastag, M., Rákhely, G., Deli, M.A., 2018. Comparison of a rat primary cell-based blood-brain barrier model with epithelial and brain endothelial cell lines: gene expression and drug transport. Front. Mol. Neurosci. 22 (11), 166.

Bors, L.A., Erdő, F., 2019. Overcoming the blood–brain barrier. challenges and tricks for CNS drug delivery. Sci. Pharm. 87 (1), 6. https://doi.org/10.3390/scipharm87010006.

Dalberto, D., Nicolau, C.C., Garcia, A.L.H., Nordin, A.P., Grivicich, I., da Silva, J., 2020. Cytotoxic and genotoxic evaluation of cotinine using human neuroblastoma cells (SH-SY5Y). Genet. Mol. Biol. 43 (2), e20190123.

Wang, F., Gao, F., Pan, S., Zhao, S., Xue, Y., 2015. Luteolin induces apoptosis, G_0/G_1 cell cycle growth arrest and mitochondrial membrane potential loss in neuroblastoma brain tumor cells. Drug Res. (Stuttg.) 65 (2), 91–95.

Romero, A., Ramos, E., Ares, I.V., Castellano, M., Martínez, M., Martínez-Larrañaga, M., Anadón, A., Martínez, M., 2017. Oxidative stress and gene expression profiling of cell death pathways in alpha-cypermethrin-treated SH-SY5Y cells. Arch. Toxicol. 91, 2151–2164.

Leone, R., Giussani, P., De Palma, S., Fania, C., Capitanio, D., Vasso, M., Brioschi, L., Riboni, L., Viani, P., Gelfi, C., 2015. Proteomic analysis of human glioblastoma cell lines differently resistant to a nitric oxide releasing agent. Mol. Biosyst 11 (6), 1612–1621.

Raszewski, G., Lemieszek, M.K., Łukawski, K., Juszczak, M., Rzeski, W., 2015. Chlorpyrifos and Cypermethrin Induce Apoptosis in HumanNeuroblastoma Cell Line SH-SY5Y. Basic Clin. Pharmacol. Toxicol. 116, 158–167.

Raszewski, G., Lemieszek, M.K., Łukawski, K., 2016. Cytotoxicity induced by cypermethrin in human neuroblastoma cell line SH-SY5Y. Ann. Agric. Environ. Med. 23 (1), 106–110.

Woehrling, E.K., Zilz, T.R., Coleman, M.D., 2006. The toxicity of hexanedione isomers in neural and astrocytic cell lines. Environ. Toxicol. Pharmacol. 22 (3), 249–254.

Krug, I., Behrens, M., Esselen, M., Humpf, H-U., 2018. Transport of enniatin B and enniatin B1 across the blood-brain barrier and hints for neurotoxic effects in cerebral cells. PLoS ONE 13 (5), e0197406.

Khan, J., Salhotra, S., Ahmad, S., Sharma, S., Abdi, S.A.H., Banerjee, B.D., Parvez, S., Gupta, S., Raisuddin, S., 2018. The protective effect of α-lipoic acid against bisphenol A-induced neurobehavioral toxicity. Neurochem. Int. 118, 166–175.

Tantarungsee, N., Yisarakun, W., Thongtan, T., Lalert, L., Srikam, S., Reuangwechvorachai, P., Ingruanglert, P., Maneesri-le Grand, S., 2018. Upregulation of pro-inflammatory cytokine expression following chronic paracetamol treatment in astrocyte. Neurotox. Res. 34 (1), 137–146.

Govindaraju, S., Rengaraj, A., Arivazhagan, R., Huh, Y.S., Yun, K., 2018. Curcumin-conjugated gold clusters for bioimaging and anticancer applications. Bioconjug. Chem. 29 (2), 363–370.

Dubuc, C., Savard, M., Bovenzi, V., Lessard, A., Côté, J., Neugebauer, W., Geha, S., Chemtob, S., Gobeil Jr., F., 2019. Antitumor activity of cell-penetrant kinin B1 receptor antagonists in human triple-negative breast cancer cells. J. Cell. Physiol. 234 (3), 2851–2865.

Choedon, T., Mathan, G., Arya, S., Kumar, V.L., Kumar, V., 2006. Anticancer and cytotoxic properties of the latex of Calotropis procera in a transgenic mouse model of hepatocellular carcinoma. World J. Gastroenterol. 12 (16), 2517–2522.

Helms, H.C., Abbott, N.J., Burek, M., Cecchelli, R., Couraud, P.O., Deli, M.A., Förster, C., Galla, H.J., Romero, I.A., Shusta, E.V., Stebbins, M.J., Vandenhaute, E., Weksler, B., Brodin, B., 2016. In vitro models of the blood-brain barrier: an overview of commonly used brain endothelial cell culture models and guidelines for their use. J. Cereb. Blood Flow Metab. 36 (5), 862–890.

Nakagawa, S., Deli, M.A., Kawaguchi, H., Shimizudani, T., Shimono, T., Kittel, A., Tanaka, K., Niwa, M., 2009. A new blood-brain barrier model using primary rat brain endothelial cells, pericytes and astrocytes. Neurochem. Int 54 (3-4), 253–263.

Cecchelli, R., Dehouck, B., Descamps, L., Fenart, L., Buée-Scherrer, VV., Duhem, C., Lundquist, S., Rentfel, M., Torpier, G., Dehouck, MP., 1999. In vitro model for evaluating drug transport across the blood-brain barrier. Adv. Drug Deliv. Rev. 36 (2-3), 165–178.

Palmgrén, JJ., Mönkkönen, J., Korjamo, T., Hassinen, A., Auriola, S., 2006. Drug adsorption to plastic containers and retention of drugs in cultured cells under in vitro conditions. Eur. J. Pharm. Biopharm. 64 (3), 369–378.

Veszelka, S., Tóth, A.E., Walter, F.R., Datki, Z., Mózes, E., Fülöp, L., Bozsó, Z., Hellinger, E., Vastag, M., Orsolits, B., Környei, Z., Penke, B., Deli, M.A., 2013. Docosahexaenoic acid reduces amyloid-β induced toxicity in cells of the neurovascular unit. J. Alzheimers Dis. 36 (3), 487–501.

Kiss, L., Hellinger, É., Pilbat, A.M., Kittel, Á., Török, Z., Füredi, A., Szakács, G., Veszelka, S., Sipos, P., Ózsvári, B., Puskás, L.G., Vastag, M., Szabó-Révész, P., Deli, M.A., 2014. Sucrose esters increase drug penetration, but do not inhibit p-glycoprotein in caco-2 intestinal epithelial cells. J. Pharm. Sci. 103 (10), 3107–3119.

Harazin, A., Bocsik, A., Barna, L., Kincses, A., Váradi, J., Fenyvesi, F., Tubak, V., Deli, M. A., Vecsernyés, M., 2018. Protection of cultured brain endothelial cells from cytokine-induced damage by α-melanocyte stimulating hormone. Peer J. 6, e4774.

Perrière, N., Demeuse, P., Garcia, E., Regina, A., Debray, M., Andreux, J.P., Couvreur, P., Scherrmann, J.M., Temsamani, J., Couraud, P.O., Deli, M.A., Roux, F., 2005. Puromycin-based purification of rat brain capillary endothelial cell cultures. Effect on the expression of blood-brain barrier-specific properties. J. Neurochem. 93 (2), 279–289.

Bocsik, A., Walter, F.R., Gyebrovszki, A., Fülöp, L., Blasig, I., Dabrowski, S., Ötvös, F., Tóth, A., Rákhely, G., Veszelka, S., Vastag, M., Szabó-Révész, P., Deli, M.A., 2016. Reversible Opening of Intercellular Junctions of Intestinal Epithelial and Brain Endothelial Cells With Tight Junction Modulator Peptides. J. Pharm. Sci. 105 (2), 754–765.

Váradi, J., Harazin, A., Fenyvesi, F., Réti-Nagy, K., Gogolák, P., Vámosi, G., Bácskay, I., Fehér, P., Ujhelyi, Z., Vasvári, G., Róka, E., Haines, D., Deli, M.A., Vecsernyés, M., 2017. Alpha-melanocyte stimulating hormone protects against cytokine-induced barrier damage in caco-2 intestinal epithelial monolayers. PLoS One 12 (1), e0170537.

Hellinger, E., Veszelka, S., Tóth, A.E., Walter, F., Kittel, A., Bakk, M.L., Tihanyi, K., Háda, V., Nakagawa, S., Duy, T.D., Niwa, M., Deli, M.A., Vastag, M., 2012. Comparison of brain capillary endothelial cell-based and epithelial (MDCK-MDR1, Caco-2, and VB-Caco-2) cell-based surrogate blood-brain barrier penetration models. Eur. J. Pharm. Biopharm. 82 (2), 340–351.